A CD22–Shp1 phosphatase axis controls integrin β7 display and B cell function in mucosal immunity

Romain Ballet [1,2 ✉], Martin Brennan[1,2,11], Carolin Brandl[3,11], Ningguo Feng[1,4,5], Jeremy Berri[1,2], Julian Cheng[1,2], Borja Ocón[1,2], Amin Alborzian Deh Sheikh [6], Alex Marki[7], Yuhan Bi[1,2], Clare L. Abram[8], Clifford A. Lowell[8], Takeshi Tsubata [6], Harry B. Greenberg[1,4,5], Matthew S. Macauley [9,10], Klaus Ley [7], Lars Nitschke[3] and Eugene C. Butcher [1,2 ✉]

The integrin $\alpha_4\beta_7$ selectively regulates lymphocyte trafficking and adhesion in the gut and gut-associated lymphoid tissue (GALT). Here, we describe unexpected involvement of the tyrosine phosphatase Shp1 and the B cell lectin CD22 (Siglec-2) in the regulation of $\alpha_4\beta_7$ surface expression and gut immunity. Shp1 selectively inhibited β_7 endocytosis, enhancing surface $\alpha_4\beta_7$ display and lymphocyte homing to GALT. In B cells, CD22 associated in a sialic acid–dependent manner with integrin β_7 on the cell surface to target intracellular Shp1 to β_7. Shp1 restrained plasma membrane β_7 phosphorylation and inhibited β_7 endocytosis without affecting β_1 integrin. B cells with reduced Shp1 activity, lacking CD22 or expressing CD22 with mutated Shp1-binding or carbohydrate-binding domains displayed parallel reductions in surface $\alpha_4\beta_7$ and in homing to GALT. Consistent with the specialized role of $\alpha_4\beta_7$ in intestinal immunity, CD22 deficiency selectively inhibited intestinal antibody and pathogen responses.

The integrin $\alpha_4\beta_7$ functions as a B and T cell adhesion receptor for the mucosal vascular addressin (mucosal addressin cell adhesion molecule 1 (MAdCAM-1)) expressed by postcapillary high endothelial venules (HEVs) in gut-associated lymphoid tissue (GALT), by lamina propria venule sites of effector cell recruitment and by stromal cells in GALT[1–3]. GALT is the major site of B cell activation and humoral immune induction for intestinal immunity. Activated B cells undergo isotype class switching in Peyer's patches (PPs) and differentiate into migratory immunoglobulin A (IgA)-secreting plasmablasts that use $\alpha_4\beta_7$ to home to mucosal surfaces[4] where local production of secretory IgA provides immune protection. Presumably in support of this role, B cells home preferentially to and predominate in murine PPs, contrasting with peripheral lymph nodes (PLNs) where T cells are the majority[5]. This homing preference correlates with higher surface expression of $\alpha_4\beta_7$ on B cells than on T cells[6], but the mechanisms responsible for this differential $\alpha_4\beta_7$ surface expression and its essential role in intestinal immunity have not been defined.

The tyrosine phosphatase Src homology region 2 domain-containing phosphatase 1 (Shp1; encoded by the gene *Ptpn6*) has essential roles in regulating immune homeostasis. Homozygous gene depletion of *Ptpn6*, as described in *motheathen* mice (*Ptpn6*[me/me]), results in severe systemic inflammation and death within weeks[7]. Closely related *motheathen viable* mutant mice (*Ptpn6*[meV/meV]) express wild-type (WT) levels of Shp1 but the catalytic activity of the enzyme is greatly reduced, resulting in a similar yet slightly less severe phenotype[8]. Shp1 plays essential roles in the regulation of tyrosine phosphorylation in T and B cells[9,10]. Shp1 can be targeted by its binding to phosphorylated immunoreceptor tyrosine-based

inhibitory motif (ITIM) sequences in membrane receptors, often acting in conjunction with ITIM-bearing molecules to inhibit signaling pathways, including those involved in integrin activity. In T cells, for example, Shp1 controls deactivation of the lymphocyte function-associated antigen 1 integrin ($\alpha_L\beta_2$) to prevent aberrant adhesion of leukocytes to β_2 integrin ligands or T cell adhesion to antigen-presenting cells[11]. In B cells, upon antigen stimulation, the phosphorylated ITIM sequences of sialic acid-binding Ig-like lectin 2 (CD22; also known as Siglec-2) recruit Shp1 to inhibit downstream components of B cell antigen receptor-induced Ca^{2+} signaling[12]. However, Shp1 has not been implicated in the control of integrin endocytosis or cell-surface expression.

Here, we report that the pair Shp1/CD22 acts in a cell-intrinsic manner to enhance $\alpha_4\beta_7$ surface abundance, with profound organotypic effects on mucosal immune responses. The findings uncover a selective role for Shp1 in $\alpha_4\beta_7$ endocytosis and surface expression, define CD22 ITIM- and lectin/carbohydrate-dependent mechanisms targeting Shp1 to β_7 integrin in B cells, and support the significance of these mechanisms to efficient intestinal antibody responses.

Results

Shp1 augments $\alpha_4\beta_7$ cell-surface display in lymphocytes. In studies of *motheaten viable* mutant mice (*Ptpn6*[meV/meV]) lacking Shp1 activity, immunofluorescence staining with antibodies to the $\alpha_4\beta_7$ heterodimer or to the β_7 subunit revealed a substantial (~90%) reduction in the median fluorescence intensity (MFI) of *Ptpn6*[meV/meV] splenic naive B cells compared with wild-type controls. The α_4 subunit, which forms heterodimers with integrin β_1 as well as β_7,
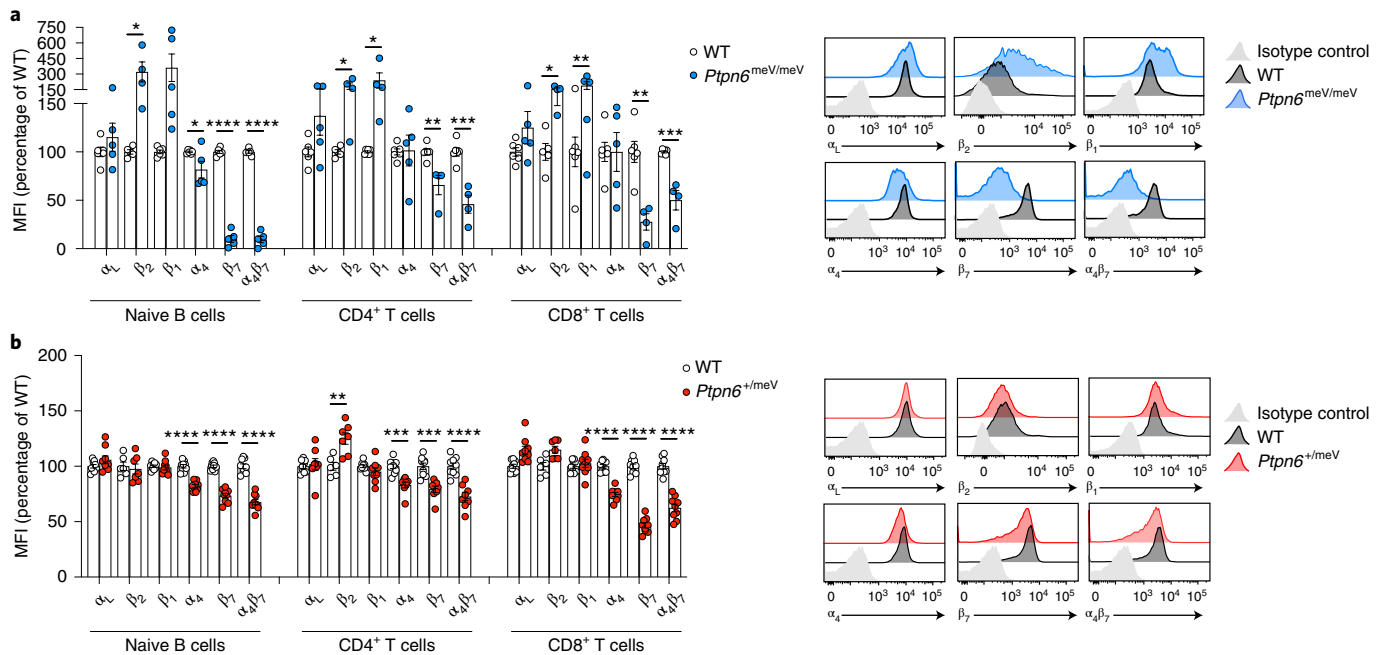
Fig. 1 | Selective reduction of integrin $\alpha_4\beta_7$ on *motheathen viable* B and T cells. a,b, Left, flow cytometry of WT versus *motheathen viable* ($Ptpn6^{meV/meV}$) (**a**) or $Ptpn6^{+/meV}$ (**b**) splenic naive B cells, CD4^{+} T cells and CD8^{+} T cells stained for α_L, β_2, β_1, α_4, β_7 or $\alpha_4\beta_7$. Shown are pooled data (means ± s.e.m.) from $n = 4$ experiments with 4–6 (**a**) or 6–9 (**b**) animals per group in total. For each animal within one experiment, the MFI of the integrin staining is expressed as a percentage of the mean MFI of the WT group. Right, representative histogram overlays gated in naive B cells. All groups were compared by two-tailed Student's t-test. *$P \leq 0.05$; **$P \leq 0.01$; ***$P \leq 0.001$; ****$P \leq 0.0001$.

was reduced ~20% in $Ptpn6^{meV/meV}$ B cells, reflecting the reduction in $\alpha_4\beta_7$. In contrast, we found no reduction for integrins α_L, β_1 and β_2 (Fig. 1a). β_7 was also reduced on CD4^{+} and CD8^{+} T cells (Fig. 1a). Since the $Ptpn6^{meV/meV}$ phenotype induces profound changes in the phenotype and homeostasis of mature B cells[13] and T cells[14,15], we repeated the above experiments with heterozygous *motheaten viable* mice ($Ptpn6^{+/meV}$). α_4, β_7 and $\alpha_4\beta_7$ integrins were also reduced on heterozygous $Ptpn6^{+/meV}$ B and T cells, while α_L, β_1 and β_2 were not affected (Fig. 1b). Thus, Shp1 positively regulates the cell-surface abundance of integrin $\alpha_4\beta_7$ on lymphocytes without affecting other integrins.

CD22 mediates Shp1-dependent $\alpha_4\beta_7$ effects in B cells. The selective effect of the $Ptpn6^{+/meV}$ phenotype on B cells suggested potential involvement of CD22, a B cell-specific lectin known to recruit Shp1 to the plasma membrane through interactions with its cytoplasmic ITIM sequences[12]. B cells from $Cd22^{-/-}$ mice showed reduced surface α_4, β_7 and $\alpha_4\beta_7$ expression by flow cytometry and confocal microscopy, but normal expression of α_L and β_1 (Fig. 2b,c,e). B cells isolated from the blood, bone marrow, PLNs and PPs of $Cd22^{-/-}$ animals displayed a similar reduction in $\alpha_4\beta_7$ (Fig. 2f). Consistent with selective expression of CD22 by B cells, CD22 deficiency had no effect on CD4^{+} T cell integrins (Extended Data Fig. 1). Messenger RNA (mRNA) expression of the β_7 subunit in wild-type and $Cd22^{-/-}$ B cells was unchanged (Fig. 2g), and subcellular imaging showed similar levels of intracellular β_7 in wild-type and mutant cells, far above cell-surface levels (Fig. 2d,e), ruling out an effect of CD22 deficiency on *Itgb7* gene expression and protein synthesis. Intracellular Shp1 spots co-localized with cell-surface β_7 in wild-type B cells more often than in $Cd22^{-/-}$ B cells (Fig. 2h,i). In wild-type cells, most of these β_7–Shp1 interactions aligned with clusters of CD22 (>80%; Fig. 2h,j).

These data suggest that CD22 mediates the Shp1 augmentation of cell-surface $\alpha_4\beta_7$. If so, we reasoned that mutation of the Shp1-binding cytoplasmic ITIM motifs in CD22 should mimic

CD22 deficiency. To address this, we used transgenic animals (CD22[Y2,5,6F]) in which the CD22 ITIM signaling domains were mutated[16] to prevent Shp1 binding and downstream CD22 signaling (Fig. 2a). B cells in CD22[Y2,5,6F] animals express normal amounts of CD22 (ref. [16]). CD22[Y2,5,6F] B cells displayed surface abundances of α_4, β_7 and $\alpha_4\beta_7$ as severely reduced as on $Cd22^{-/-}$ B cells, again with no effect on the α_L or β_1 integrin surface expression (Fig. 2b).

CD22 is a lectin that interacts in *cis* with α2-6-sialic acid (α2-6-Sia)-decorated glycoproteins such as CD22 (ref. [17]) or CD45 (ref. [18]), affecting its distribution and motility on the B cell surface[19]. To assess a potential role for the CD22 lectin–carbohydrate interactions in cell-autonomous $\alpha_4\beta_7$ regulation, we assessed the integrin cell-surface levels of B cells expressing a mutated lectin domain (CD22[R130E]) that prevents α2-6-Sia binding[16] (Fig. 2a). CD22[R130E] B cells expressed CD22 at wild-type levels[16] and displayed a significant reduction in $\alpha_4\beta_7$ levels (Fig. 2b), although the effect was less severe than that of CD22 deficiency or ITIM mutations. Intermediate reduction in $\alpha_4\beta_7$ was also observed in B cells from $St6Gal1^{-/-}$ mice, which lack α2,6-sialyltransferase activity[20] and thus CD22 ligands (Extended Data Fig. 2).

α2-6-Sia-dependent CD22–β_7 association at the cell surface. The reduction of β_7 in the absence of CD22 lectin activity suggests cell-surface interactions between CD22 and β_7. Using proximity ligation assay (PLA) in resting B cells, we detected a robust PLA signal between CD22 and β_7 (~5–6 spots per cell; Fig. 3a), but there was no interaction of CD22 and β_1 (Fig. 3b). A strong CD22-independent PLA signal was observed with anti-β_1 and anti-α_4 antibodies (detecting $\alpha_4\beta_1$ heterodimer interactions), confirming the activity and specificity of the β_1 antibody (Fig. 3c). To assess dependence on sialic acid, we pre-treated purified B cells with *Arthrobacter ureafaciens* sialidase at a concentration that retained cell viability while reducing *Sambucus nigra* lectin (α2-6-Sia-binding lectin) staining by ~60% (Extended Data Fig. 3). Sialidase-treated wild-type B cells showed significantly reduced association between CD22 and β_7
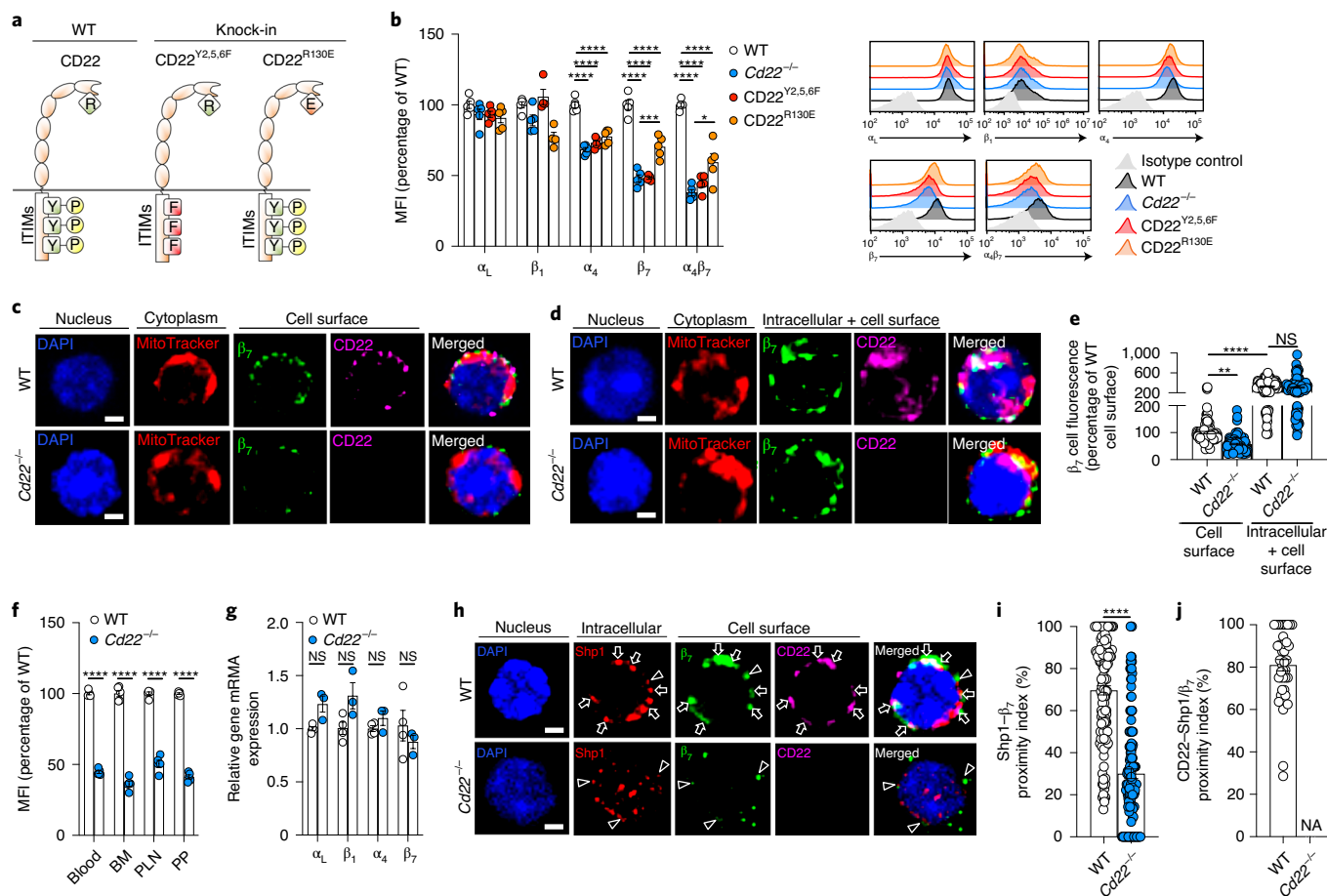
Fig. 2 | CD22 mediates Shp1-dependent $\alpha_4\beta_7$ augmentation in B cells. a, Schematic of WT CD22, CD22^{Y2,5,6F} and CD22^{R130E} mutants. **b**, Left, flow cytometry of WT and CD22 mutant splenic B cells stained for α_L, β_1, α_4, β_7 or $\alpha_4\beta_7$. Shown are pooled data (means ± s.e.m.) from $n = 3$ experiments with 7 animals per group in total, analyzed and presented as in Fig. 1. Right, representative histogram overlays gated in naive B cells. **c,d**, Immunofluorescence staining of cell-surface (**c**) and intracellular + cell-surface (**d**) β_7 and CD22 in B cells. The nucleus, cytoplasm, β_7 and CD22 are stained blue (DAPI), red (MitoTracker Deep Red), green and magenta, respectively. Scale bars, 2 μM. **e**, For each cell shown in **c** and **d**, we quantified the intensity of the β_7 fluorescence. Shown are pooled data (means ± s.e.m.) from three independent experiments, with ~100 cells in total analyzed per condition. The mean β_7 fluorescence intensity for the WT cell-surface group was set to 100 and the data are shown as a percentage of this total. NS, not significant. **f**, Flow cytometry of WT or $Cd22^{-/-}$ B cells isolated from blood, bone marrow (BM), PLNs and PPs and stained for $\alpha_4\beta_7$ or isotype-matched control. Shown are pooled data (means ± s.e.m.) from $n = 2$ independent experiments, with five animals per group in total. **g**, mRNA expression of α_L, β_1, α_4 and β_7 integrins in B cells from WT and $Cd22^{-/-}$ mice. Shown are pooled data (means ± s.e.m.) from two independent experiments with 3–4 animals per group in total. **h**, Immunofluorescence staining of intracellular Shp1 and cell-surface β_7 and CD22 in B cells. The nucleus, Shp1, β_7 and CD22 are stained blue (DAPI), red, green and magenta, respectively. The arrowheads show Shp1–β_7 colocalization and the arrows show CD22–Shp1/β_7 colocalization. **i,j**, For each cell shown in **h**, we calculated Shp1–β_7 (**i**) and CD22–Shp1/β_7 (**j**) proximity indices (see Methods). Shown are pooled data (means ± s.e.m.) from two independent experiments, with 130 (**i**) and 40 (**j**) cells in total analyzed per condition. Groups were compared by one-way ANOVA with Dunnett's multiple comparisons test (**b** and **e**) or two-tailed Student's t-test (**f**, **g** and **i**). NA, not applicable. *$P \leq 0.05$; **$P \leq 0.01$; ***$P \leq 0.001$; ****$P \leq 0.0001$.

compared with untreated wild-type cells (Fig. 3a). Together, these data show a cell-surface sialic acid-dependent CD22 association with integrin β_7 but not β_1.

CD22–Shp1 inhibits β_7 endocytosis in B cells. Cell-surface receptor expression is regulated by endocytosis and recycling[21]. We compared the effects of CD22 or Shp1 deficiency on endocytosis of β_7 versus β_1 integrins and of the transferrin receptor as a control that undergoes endocytic recycling. We assessed internalization by flow cytometry using pHrodo Red, a dye whose fluorescence increases within the acidic pH of endocytic vesicles. We incubated splenocytes at 37 °C to enable endocytosis in the presence of pHrodo Red-conjugated transferrin, anti-β_7, anti-β_1 or isotype-matched control antibodies. The background was defined by staining of cells with the pHrodo Red constructs incubated at 4 °C to prevent

endocytosis. Endocytosis, defined by the internalization-induced (background-corrected) pHrodo Red signal, was normalized to the cell-surface expression of each antigen at 4 °C to yield a relative endocytosis ratio (RER; Fig. 4a).

CD22-deficient B cells displayed a significantly higher RER for integrin β_7 compared with wild-type B cells (1.65-fold higher; $P < 0.0001$). CD22 deficiency did not alter the basal endocytosis of transferrin or integrin β_1 (Fig. 4b), and endocytosis was not observed for the isotype control antibodies (data not shown). $Ptpn6^{+/meV}$ B cells showed a shift similar to that of $Cd22^{-/-}$ cells, but not reaching significance. Treatment of cells with primaquine, to inhibit recycling of proteins back to the plasma membrane[22], increased internalization. It also increased the differences between the RERs of the following versus wild-type B cells (RER = 1.18): $Ptpn6^{+/meV}$ (RER = 1.54; $P < 0.05$); $St6Gal1^{-/-}$ (RER = 1.59; $P < 0.01$);
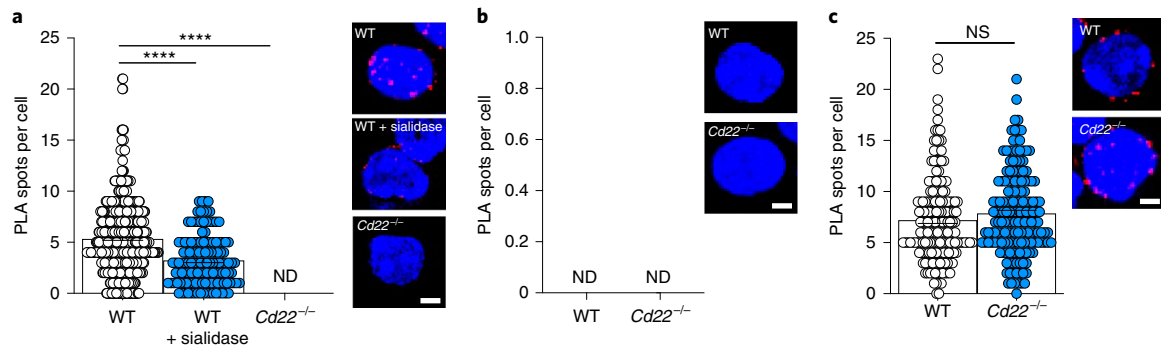
Fig. 3 | Direct physical association of CD22 and β7. a, Association between CD22 and integrin β7 was assessed by PLA using purified B cells from either untreated or sialidase-treated WT animals, or $Cd22^{-/-}$ animals. **b**, Association between CD22 and integrin β1 was assessed as a negative integrin control. **c**, Association between α4 and β1 was analyzed as a positive control for the β1 integrin. In **a**–**c**, pooled data (means ± s.e.m.) from two independent experiments are shown, with ~200–400 cells analyzed per condition in total. Inset: immunofluorescence stains. Scale bars, 2 μM. Groups were compared by one-way ANOVA with Dunnett's multiple comparison test (**a**) or two-tailed Student's t-test (**c**). ****$P \leq 0.0001$. ND, not detectable.
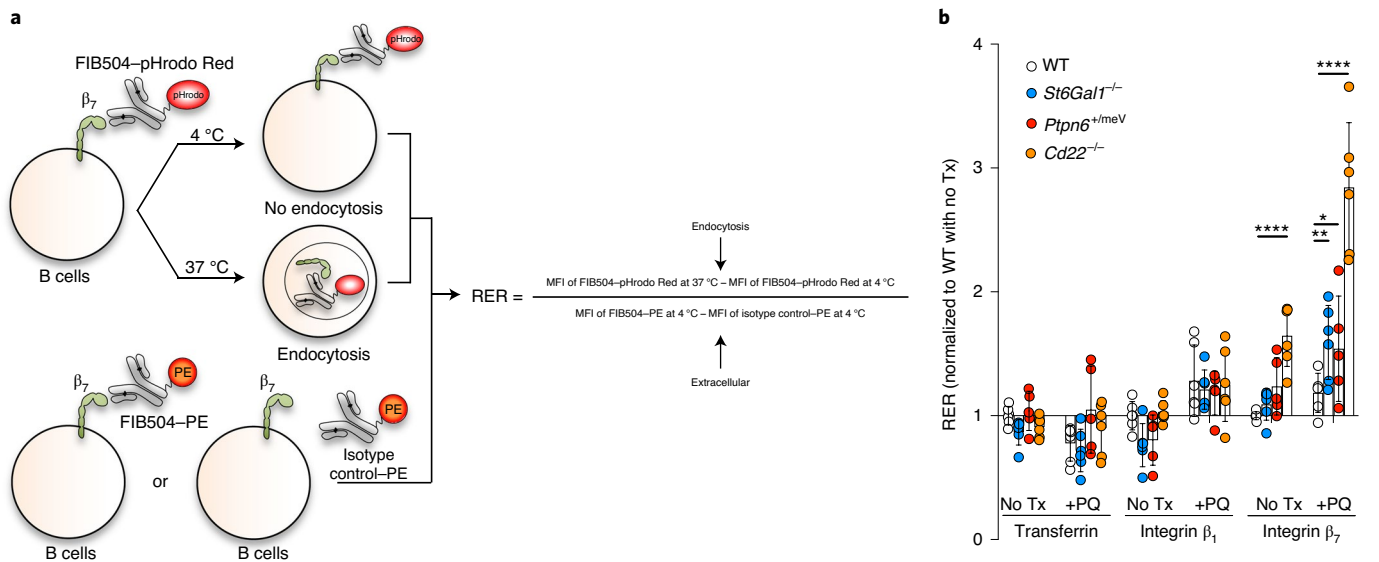

Fig. 4 | CD22 limits integrin β7 endocytosis in B cells via Shp1 and ligand recognition. a, Splenocyte staining with anti-CD19 and anti-IgD (to identify B cells) and pHrodo Red-conjugated tranferrin, HMβ1-1 (anti-β7) or FIB504 (anti-β7) antibodies at either 4 °C (no endocytosis) or 37 °C (endocytosis) was used to calculate endocytosis levels (that is, the MFI of pHrodo Red staining at 37 °C minus the MFI of pHrodo Red staining at 4 °C). Staining at 4 °C with phycoerythrin (PE)-conjugated RI7217 (anti-transferrin receptor 1, (TfR1)), HMβ1-1, FIB504 or the matching phycoerythrin-conjugated isotype control antibodies was used to calculate extracellular TfR1, β1 and β7 levels (that is, the MFI of the antigen-specific phycoerythrin staining at 4 °C minus the MFI of isotype control-phycoerythrin staining at 4 °C). For each molecule (illustrated with β7 in **a**) and each experiment, the RER was calculated by normalizing endocytosis levels to extracellular levels. **b**, RER of transferrin, β1 and β7 in WT, $St6Gal1^{-/-}$, $Ptpn6^{+/meV}$ and $Cd22^{-/-}$ B cells with (+PQ) or without (no Tx) 100 μM primaquine treatment. The mean RER of the WT B cells group without primaquine was set to 1 and all data were normalized to that mean value. Shown are pooled data (means ± s.e.m.) from $n = 3$ independent experiments, with 6 animals per group in total. All groups were compared by two-way ANOVA with Šidák's multiple comparisons test. *$P \leq 0.05$; **$P \leq 0.01$; ****$P \leq 0.0001$.

and $Cd22^{-/-}$ (RER = 2.84; $P < 0.0001$) (Fig. 4b). These results suggest that loss of CD22 or reduction of Shp1 activity ($Ptpn6^{+/meV}$) similarly and selectively inhibit β7 endocytosis in B cells.

CD22–Shp1 restrains plasma membrane β7 phosphorylation.
Integrin β tails, including that of β7, comprise conserved motifs for tyrosine phosphorylation by Src family kinases, regulating integrin functions[23–25]. These motifs interact with a large number of phosphotyrosine-binding (PTB) domain-containing proteins, including proteins that regulate endocytic trafficking[25–28]. To determine whether CD22 restrains phosphorylation of β7 at the cell surface, we compared tyrosine phosphorylation of cell-surface

versus intracellular β7 in CD22-deficient versus wild-type B cells. We biotinylated cell-surface proteins by incubation of cells with Sulfo-NHS-Biotin at 4 °C to prevent protein internalization (Fig. 5a). We isolated cell-surface β7 from purified B or T cell lysate using successive immunoprecipitations for β7 with the β7-specific antibody FIB504 and then for biotin with streptavidin-conjugated beads (SA-IP). We recovered cell-surface β7 from the eluate of the SA-IP and intracellular β7 from the biotin-free flowthrough before quantification of β7 and phosphotyrosine (p-Tyr) by immunoblot (Fig. 5a). We found a significant increase of p-Tyr (normalized to β7) in the cell-surface β7 fraction of $Ptpn6^{+/meV}$ and $Cd22^{-/-}$ B cells compared with wild-type controls, whereas phosphorylation of intracellular β7
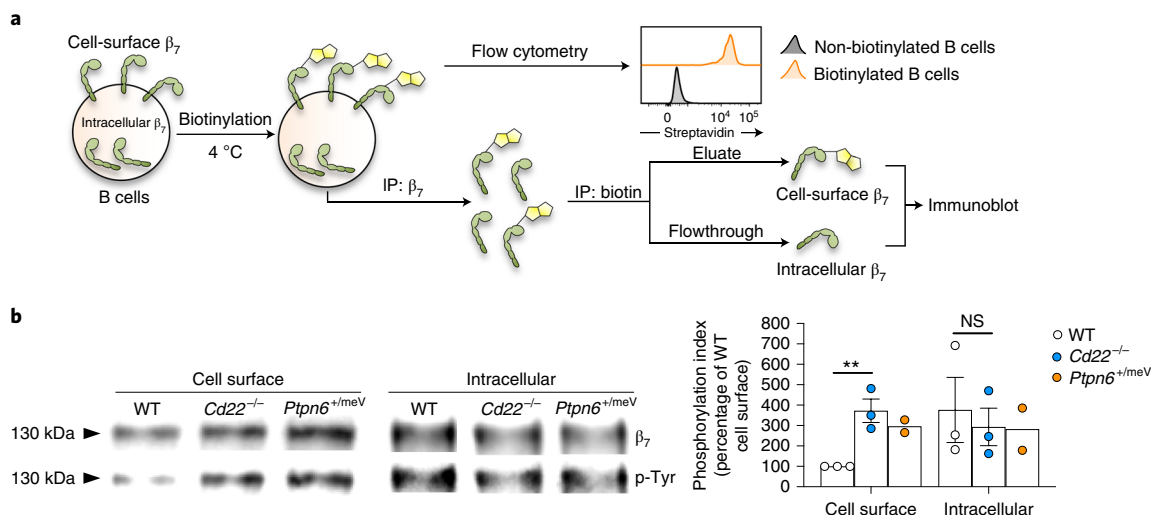
Fig. 5 | CD22 restrains tyrosine phosphorylation of cell-surface β₇ integrin in B cells. a, Schematic of the double immunoprecipitation (IP) experiment. Cell-surface proteins of purified naive B cells were biotinylated with Sulfo-NHS-Biotin at 4 °C for 1 h. Biotinylation was confirmed by flow cytometry using a streptavidin-conjugated probe. Biotinylated B cell lysate was used for immunoprecipitation of β₇ integrin (including biotinylated cell-surface β₇ and biotin-free intracellular β₇). Following elution for β₇, a second immunoprecipitation with streptavidin beads was used to recover cell-surface β₇ (eluate of the SA-IP) from intracellular β₇ (flowthrough of the SA-IP) before immunoblot studies. **b**, Left, detection of β₇ and p-Tyr levels in cell-surface and intracellular β₇ fractions (130 kDa) of WT, CD22-deficient (*Cd22*⁻/⁻) and *Ptpn6*⁺/ᵐᵉⱽ B cells after the double immunoprecipitation shown in **a**. Right, quantification of p-Tyr levels normalized to β₇ levels (p-Tyr:β₇ ratio). Within each experiment, the p-Tyr:β₇ of the cell-surface β₇ of the WT group was set to 100, and the data are expressed as a percentage of this total. Shown are pooled data (means ± s.e.m.) from n = 2–3 independent experiments. Each dot represents one independent experiment with n = 8 pooled animals for WT and *Cd22*⁻/⁻ (that is, n = 24 animals in total for n = 3 independent experimental replicates) and n = 4 pooled animals for *Ptpn6*⁺/ᵐᵉⱽ (that is, n = 8 animals in total for n = 2 experimental replicates). The data were analyzed by two-tailed Student's t-test. **P ≤ 0.01.

did not differ in mutant versus wild-type cells (Fig. 5b). The p-Tyr:β₇ ratio among the cell-surface β₇ fraction of *Ptpn6*⁺/ᵐᵉⱽ and *Cd22*⁻/⁻ B cells reached levels similar to the intracellular pool. In contrast with the effects of CD22 deficiency on surface β₇ phosphorylation in B cells, we found no difference in cell-surface p-Tyr:β₇ ratios in *Cd22*⁻/⁻ T cells compared with wild-type T cells (Extended Data Fig. 4). In conjunction with the known role of phosphorylation in endocytosis, these results suggest that tyrosine phosphorylation of β₇ at the cell surface functions as a switch to enhance β₇ endocytosis and that the CD22–Shp1 axis shifts the balance of p-Tyr towards β₇ dephosphorylation to maintain the integrin at the cell surface.

CD22–Shp1 enhances B cell homing to GALT. To assess the consequence of CD22–Shp1-dependent α₄β₇ regulation in GALT, we first assessed the lymphocyte composition of *Cd22*⁻/⁻ and wild-type PPs. PPs from mutant and wild-type animals were similar in number and size (Fig. 6a), but mutant PPs had a significant decrease (~70%) in naive B cell numbers compared with wild-type PPs (Fig. 6b). There was no difference in germinal center or activated B cells (CD19⁺IgD⁻) or T cell numbers (Fig. 6b and Extended Data Fig. 5). We found no difference in the PLNs, taken as controls, showing the specificity of the effects for GALT (Fig. 6b).

Next, we assessed the short-term homing of mutant B cells into PPs and mesenteric lymph nodes (MLNs), which express the dedicated α₄β₇ ligand MAdCAM-1. Recipient wild-type mice received splenocytes from wild-type and mutant donors labeled with different CellTracker dyes and mixed at a 1:1:1 ratio, as confirmed by flow cytometry. Two hours later, we established the cells localized to PPs and MLNs by flow cytometry (Fig. 6c). In agreement with the reduction of α₄β₇, *Ptpn6*⁺/ᵐᵉⱽ B cells, *Cd22*⁻/⁻ B cells, CD22^Y2,5,6F ITIM mutant B cells and CD22^R130E lectin mutant B cells homed poorly to PPs, displaying a similar ~60% reduction in recruitment compared with wild-type B cells (Fig. 6d,e). We observed an intermediate defect for all mutant B cells in homing to the MLN that was consis-

tent with MAdCAM-1 expression on subsets of MLN HEVs, while homing to the PLNs, spleen and bone marrow, which is independent of α₄β₇, was normal (Fig. 6d,e and Extended Data Fig. 6). CD22 deficiency did not affect CD4⁺ T cell homing to PPs, while reduced Shp1 activity (*Ptpn6*⁺/ᵐᵉⱽ) compromised CD4⁺ T cell homing, consistent with reduced cell-surface β₇ expression. *Ptpn6*⁺/ᵐᵉⱽ CD4⁺ T cells also localized poorly to PLNs (Extended Data Fig. 7). This may reflect the role of Shp1 in modulating β₂ integrin activity in T cells[11].

α₄β₇ mediates activation-independent tethering and rolling on PP, as well as chemokine/integrin activation-dependent arrest in combination with lymphocyte function-associated antigen 1 (ref. [2]). To assess the effects of the CD22–Shp1 axis on these steps, we visualized B and T cell behavior in PPs by intravital microscopy. We purified B or T cells from wild-type, *Ptpn6*⁺/ᵐᵉⱽ and *Cd22*⁻/⁻ donors, labeled them with different CellTracker dyes, mixed mutant and wild-type cells at a 1:1 ratio (as confirmed by flow cytometry) and transferred the cells into a recipient wild-type mouse while imaging one PP (Fig. 6f). We captured high-frame-rate videos (40 frames per second) to study the behavior of all cells entering HEVs within the field of view during the recording (~30–40 s). We stratified the cells into four groups (that is, flyers, brief rollers, rollers and arresters) based on their interactions with HEVs. Freely flowing cells that failed to interact detectably, termed flyers, appeared as streaks due to their high velocity during the time of exposure, and passed through the HEVs at a mean velocity of ~1,000 μm s⁻¹ (Extended Data Fig. 8a–c and Supplementary Video 1). Cell capture on the vessel wall could be visualized as soon as the cell appeared round and bright as a result of reduced velocity. Cells attaching briefly (<1 s) before detaching and flying through the HEV were described as brief rollers (Extended Data Fig. 8b,c and Supplementary Video 2). Cells interacting for more than 1 s were called rollers (Extended Data Fig. 8b,c and Supplementary Video 3). Among rollers, cells static for more than 2 s at the end of the recording were considered arresters.

At the end of ~30 s of observation, the numbers of $Ptpn6^{+/meV}$ and $Cd22^{-/-}$ arrested B cells were ~50 and ~60% lower, respectively ($P < 0.0001$), than wild-type B cells (Fig. 6g,j and Supplementary Videos 4 and 5). The reduced frequency of arrest correlated with inefficient initial capture or tethering, as well as faster rolling (looser interaction) of $Ptpn6^{+/meV}$ and $Cd22^{-/-}$ B cells. We observed a reduced frequency of rolling by $Ptpn6^{+/meV}$ and $Cd22^{-/-}$ B cells compared with wild-type control cells, with a corresponding increase in non-interacting flyers (Fig. 6h,k). Among rollers, the average rolling velocity of $Ptpn6^{+/meV}$ and $Cd22^{-/-}$ B cells was ~2–3 times higher than wild-type controls (Fig. 6i,l and Supplementary Videos 6 and 7). The total number of mutant cells and wild-type B cells entering PP HEVs (including rollers, brief rollers or flyers) was similar in each experiment, thus ruling out distortion of the results by differences in the retention of mutant cells in other organs (Extended Data Fig. 8d). The CD22 effect could be due to a lack of interaction with the HEV-expressed CD22 ligand: however, the parallel alterations in $Ptpn6^{+/meV}$ B cell behavior suggest that the cell-intrinsic reduction of $\alpha_4\beta_7$, which $Ptpn6^{+/meV}$ and CD22-deficient B cells have in common, is probably the major factor involved in reduced interaction efficiency and PP homing. Consistent with this hypothesis, the effects of CD22 deficiency and reduced Shp1 activity ($Ptpn6^{+/meV}$) on both tethering and rolling velocity were phenocopied by experimental reduction in the surface $\alpha_4\beta_7$ available for interaction (Extended Data Fig. 9). Moreover, reduced $\alpha_4\beta_7$ on $Cd22^{-/-}$ B cells significantly impacted homing to the PP, even in absence of the CD22 ligand on PP HEVs (Extended Data Fig. 10).

We conclude that Shp1-driven CD22 regulation of β_7 drives enhanced B cell homing to GALT and substantially augments the adhesive functions of the mucosal lymphocyte integrin $\alpha_4\beta_7$.

CD22 deficiency inhibits intestinal antibody responses. In addition to its roles in gut lymphocyte homing, $\alpha_4\beta_7$ mediates cell–cell interactions of lymphocytes with MAdCAM-1 expressed by follicular dendritic cells in GALT[29]. It also supports interactions of $\alpha_4\beta_7$-expressing lymphocytes with other ligands, including α_4 on adjacent immune cells, fibronectin in the extracellular matrix, and vascular cell adhesion molecule 1 (refs. [1,30]). Moreover, $\alpha_4\beta_7$ is highly expressed by B cells involved in gut immune responses, but is downregulated on B cells responding to systemic (non-intestinal) antigens[31–33]. Thus, we reasoned that CD22-dependent $\alpha_4\beta_7$ surface expression might have a selective role in intestinal (versus systemic) antibody responses. In contrast, CD22 suppresses B cell antigen receptor responses in general, and its deficiency has been considered to enhance B cell activation.

To distinguish between these possibilities, we immunized wild-type and CD22-deficient mice with cholera toxin B (CTB) by different routes and compared the humoral responses 2 weeks later.

CD22 deficiency caused a clear reduction in antigen-specific IgA and IgG responses to oral CTB, but not to nasal or intramuscular immunization (Fig. 7a,c). Total IgA and IgG concentrations in the serum after oral, nasal and intramuscular immunizations were similar in CD22-deficient versus wild-type animals, ruling out global inhibition or activation of B cell responses (Fig. 7b,d).

We also analyzed CTB-specific IgA and IgG production from ex vivo cultures of small intestine segments. Intestinal CTB-specific IgA (Fig. 7e) and IgG (Fig. 7f) were decreased in $Cd22^{-/-}$ mice after oral immunization, and CTB-specific IgA was decreased after intramuscular immunization, but there was no significant alteration in small intestine IgA or IgG after intranasal immunization (Fig. 7e,f). These results suggest that the CD22-driven augmentation of $\alpha_4\beta_7$ surface expression selectively amplifies gut-specific, but not systemic, antibody responses.

CD22 improves the antibody response to rotavirus (RV). RV selectively infects intestinal epithelial cells, leading to strong immune responses in GALT, and the local production of RV-specific IgA plays an important role in protection[34]. Young pups, which are more susceptible to infection than adults, were infected with RV. We measured total and RV-specific IgA and IgG in the feces daily. Ten days post-infection, wild-type animals started to mount robust RV-specific intestinal IgA and IgG responses (Fig. 8a,b), which preceded a reduction of fecal viral shedding by day 12 post-infection and a full resolution of RV infection by day 15 post-infection (Fig. 8c). In contrast, CD22-deficient animals had a dramatically reduced RV-specific IgA response in the feces (Fig. 8a) and a delay in the resolution, as indicated by residual viral shedding at day 12 post-infection (Fig. 8c). Virus was eliminated by day 15 post-infection in both wild-type and $Cd22^{-/-}$ mice (Fig. 8c).

At the peak of the fecal antibody response (day 12 post-infection), we observed reduced RV-specific IgA titers in the serum of CD22-deficient animals (Fig. 8d), while RV-specific IgG, total IgG and total IgA titers were similar to those in wild-type animals (Fig. 8d,e). $Cd22^{-/-}$ animals also had fewer RV-specific IgA antibody-secreting B cells in MLNs and the small intestine lamina propria than wild-type mice at day 12 post-infection, while there were no differences in the spleen (Fig. 8f). To determine whether the reduction of RV-specific fecal antibody in $Cd22^{-/-}$ mice reflected a deficit in local production in the gut (as opposed to altered antibody secretion in bile), we analyzed RV-specific IgA and IgG levels in ex vivo culture of small intestine segments. We found a twofold decrease in the RV-specific IgA and IgG titers in CD22-deficient animals compared with wild-type controls (Figs. 8g and 8h), which correlated with higher viral shedding in the feces at day 12 post-infection, as mentioned above (Fig. 8c). Together, these data

Fig. 6 | Functional assays reveal defective PP homing and altered endothelial interactions of $Ptpn6^{+/meV}$ and $Cd22^{-/-}$ B cells. a, Numbers of PPs in WT and $Cd22^{-/-}$ B cells. Shown are pooled data (means ± s.e.m.) from $n = 2$ experiments with 8 mice per group in total. Inset: representative images of WT and $Cd22^{-/-}$ PPs, indicated by arrowheads. Scale bars, 2 mm. **b**, Numbers of germinal center/activated B cells (GC/A; CD19$^+$IgD$^-$) and naive B cells (CD19$^+$IgD$^+$) in MLNs, PLNs and PPs of WT and $Cd22^{-/-}$ animals, shown as a percentage of the mean of the WT group. Shown are pooled data (means ± s.e.m.) of $n = 2$ experiments with 11–12 mice per group in total. **c**, Schematic of the short-term homing assay. i.v., intravenous. **d,e**, Left, localization of WT, $Cd22^{-/-}$ and $Ptpn6^{+/meV}$ B cells (**d**) or WT, $Cd22^{-/-}$, CD22^{Y2,5,6F} and CD22^{R130E} B cells (**e**) in PLNs, MLNs and PPs after homing assays. The data are shown as a percentage of the mean localization ratio of the WT group. Shown are pooled data (means ± s.e.m.) of $n = 3$–5 experiments, with 11–16 mice per group in total. Right, representative dot plots gated on naive B cells. **f**, Schematic of the in situ video microscopy experiment. Representative video stills are shown of WT B cells (green) and $Ptpn6^{+/meV}$ cells (red). Scale bar, 100 µm. **g,j**, Numbers of WT versus $Ptpn6^{+/meV}$ (**g**) or $Cd22^{-/-}$ (**j**) arresters on PP HEVs were counted per second from the first cell entering the HEVs. The total number of WT B cell arresters at the end of each experiment (that is, the WT maximum; ~40–80 cells on average) was set to 100 and the data are expressed as a percentage of this total. **h,k**, The behavior (that is, flyer, brief roller or roller; as defined in Extended Data Fig. 8) of WT versus $Ptpn6^{+/meV}$ (**h**) or $Cd22^{-/-}$ cells (**k**) entering the HEVs was analyzed in 3–4 representative PP HEVs per experiment. The results are shown as a percentage of the total number of cells entering HEVs (~250–300 cells were analyzed per group). The data in **g**, **h**, **j** and **k** represent means ± s.e.m. of three independent experiments. **i,l**, Average rolling velocities (means ± s.e.m.) of representative $Ptpn6^{+/meV}$ (**i**) or $Cd22^{-/-}$ roller cells (**l**) versus WT cells from $n = 3$ experiments. Groups were compared by two-tailed Student's t-test (**a**, **b**, **h**, **i**, **k** and **l**), one-way ANOVA with Dunnett's multiple comparisons test (**d** and **e**) or paired two-tailed Student's t-test (**g** and **j**). *$P \leq 0.05$; **$P \leq 0.01$; ***$P \leq 0.001$; ****$P \leq 0.0001$.

highlight a substantial role of B cell CD22 in the mucosal pathogen response.

Discussion

We report a previously unappreciated contribution for the CD22–Shp1 complex in cell-autonomous regulation of the gut integrin receptor $\alpha_4\beta_7$. We show that Shp1 inhibits $\alpha_4\beta_7$ endocytosis and maintains cell-surface $\alpha_4\beta_7$ expression. We show that B cell-specific Shp1-binding lectin CD22 associates with β_7 on the cell surface,

specifically targeting Shp1 to β_7 and reducing β_7 tyrosine phosphorylation. Our results support a model in which this cascade inhibits $\alpha_4\beta_7$ endocytosis and degradation, resulting in higher surface expression of the gut-homing integrin. We present evidence that this novel mechanistic cascade is functionally important not only in B cell homing to GALT but also in intestinal antibody responses. These results define a novel pathway for differential control of integrin function and an unexpected and selective role for a CD22–Shp1 axis in intestinal immunity.
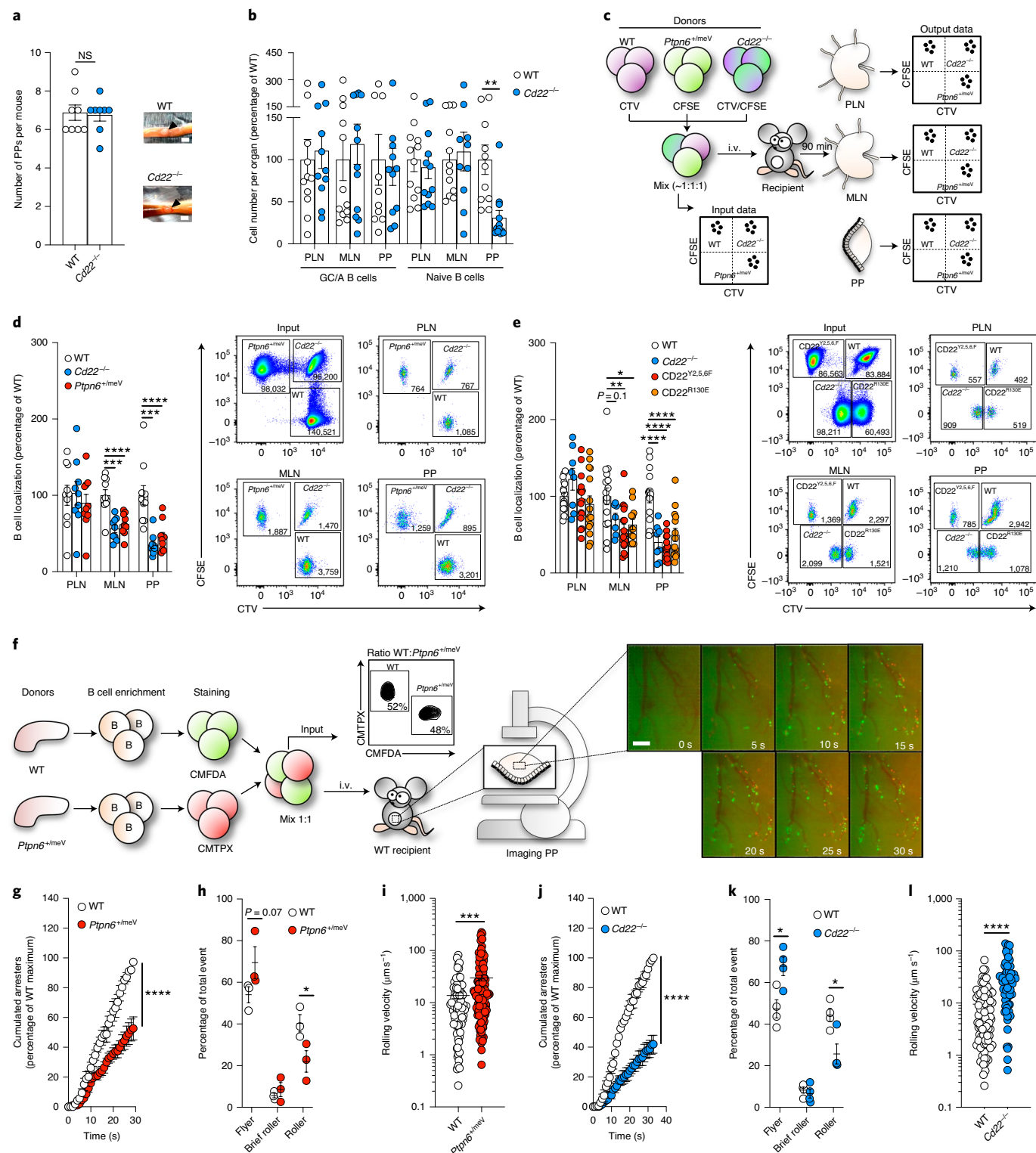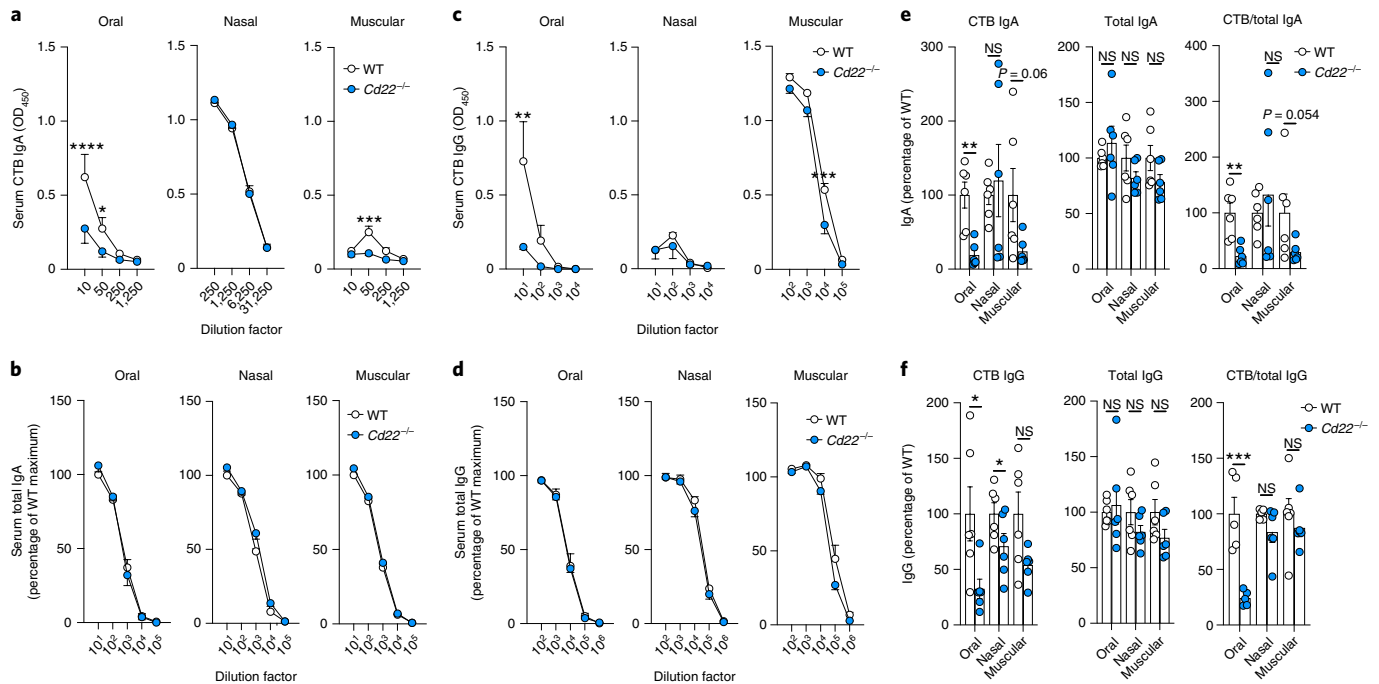
Fig. 7 | Defects in intestinal responses to oral antigen in CD22-deficient mice. Cohorts of WT or $Cd22^{-/-}$ mice were immunized with CTB via the oral, intranasal (nasal), or intramuscular (muscular) route for 2 weeks. **a–d**, Serum levels of CTB-specific IgA (**a**), total IgA (**b**), CTB-specific IgG (**c**) and total IgG (**d**) as measured by ELISA and expressed as the net OD_{450} or a percentage of the mean OD_{450} measured in the lowest dilution factor of the WT group. **e,f**, Small intestine segments were cultured ex vivo for 3 days to titer the quantity of secreted CTB-specific IgA, total IgA and CTB-specific IgA normalized to total IgA (**e**) or CTB-specific IgG, total IgG and CTB-specific IgG normalized to total IgG (**f**) produced by ELISA and expressed as a percentage of the WT group mean. Shown in **a–f** are pooled data (means ± s.e.m.) from $n = 2$ experiments, with 5–6 mice per group in total. Groups were compared by two-way ANOVA with Šidák's multiple comparisons test (**a–d**) or two-tailed Student's t-test (**e** and **f**). $*P \leq 0.05$; $**P \leq 0.01$; $***P \leq 0.001$; $****P \leq 0.0001$.

β integrin phosphorylation controls integrin functions including activation[23,25,35] and endocytosis[28,36,37] by means of PTB domain-containing proteins that interact with integrin β tails such as talin[38], kindlin[38], Dok-1 (refs. [23–25]) or phox homology band 4.1/ezrin/radixin/moesin (PX-FERM) domain-containing sorting nexins[39,40]. Our results suggest that Shp1 acts as a phosphorylation switch that directly or indirectly restrains tyrosine phosphorylation of integrin β_7, thus reducing β_7 endocytosis. On B cells, CD22 targeting of Shp1 to β_7 may also alter the phosphorylation state of other PTB domain- or FERM domain-containing targets in the vicinity of the integrin, potentially affecting endocytic adaptors[37] to inhibit endocytosis as well.

β_7 cell-surface levels in $Cd22^{-/-}$ B cells are comparable to those on wild-type naive T cells, suggesting that CD22 itself is enough to explain the higher surface expression of $\alpha_4\beta_7$ by normal naive B versus T cells[6]. It is intriguing to speculate that alternative ITIM-containing proteins may regulate T cell β_7, perhaps contributing to the enhanced β_7 display by intestinal memory T cells.

On B cells, CD22 can associate in *cis* with α2-6-Sia-modified membrane glycoproteins, including CD22 itself and CD45. These *cis* interactions can bring ITIM-bound Shp1 phosphatase into close proximity to target substrates, altering the phosphorylation state and function of associated molecules[12]. Using PLAs, we showed that β_7 but not β_1 integrin associates closely with CD22, a specific interaction that is dependent on cell-surface sialic acid and that probably contributes to the magnitude and specificity of the effects. Yet, the reduction of β_7 in lectin- (CD22[R130E]) and St6gal1-deficient cells was less than that in CD22[Y2,5,6F] cells with mutated CD22 ITIMs. In CD22[R130E] B cells, CD22 itself is known to be more phosphorylated, to recruit more Shp1 and to have higher lateral mobility than in wild-type B cells[16,19]. These effects would be expected to allow CD22–Shp1 to access β_7 even in the absence of specific targeting, explaining the partial retention of surface levels in the absence of

lectin activity (CD22[R130E]) or CD22 ligand ($St6gal1^{-/-}$), as well as the intermediate effect on endocytosis seen with $St6Gal1^{-/-}$ B cells. Taken together, these data suggest that CD22−α2-6-Sia interactions recruit CD22−ITIM-docked Shp1 phosphatase to β_7 to alter the local tyrosine phosphorylation balance, inhibit β_7 endocytosis and enhance $\alpha_4\beta_7$ surface expression.

B cell positioning, activation and cell−cell interactions in the GALT, which all involve contributions from $\alpha_4\beta_7$, drive the production of local and systemic antibodies to intestinal antigens and pathogens. Although CD22-deficient mice show grossly normal systemic B cell development[41], we observed a profound defect in the intestinal and systemic antigen-specific IgA and IgG levels in response to oral immunization with CTB in CD22-deficient animals, whereas the IgG response to nasal or intramuscular immunization was preserved. These results closely recapitulate the reported effects of β_7 deficiency or $\alpha_4\beta_7$ blockade, which also selectively impair antibody responses to oral versus systemic antigen[42]. Taking into account that CD22 is known to restrain B cell responses and that its deficiency may enhance them in vivo[43], the selective reduction of mucosal immune responses in CD22-deficient animals highlights the critical and dominant importance of the CD22-dependent β_7 regulation for optimum mucosal immunity. Accordingly, we found that CD22 deficiency impaired the response of mice to infection with RV, a reovirus that selectively infects small intestinal epithelial cells and is a major cause of childhood diarrheal illness[44]. CD22 deficiency caused a significant reduction in viral clearance comparable to that reported in mice with a complete lack of B cells[45], or lacking IgA[46] or GALT[47] itself. The protective effect of CD22 deficiency probably reflects global influences of CD22-dependent $\alpha_4\beta_7$ functions in the intestinal immune response.

We previously showed that PP and MLN HEVs, but not PLN HEVs, express functional carbohydrate ligands for CD22 encoded
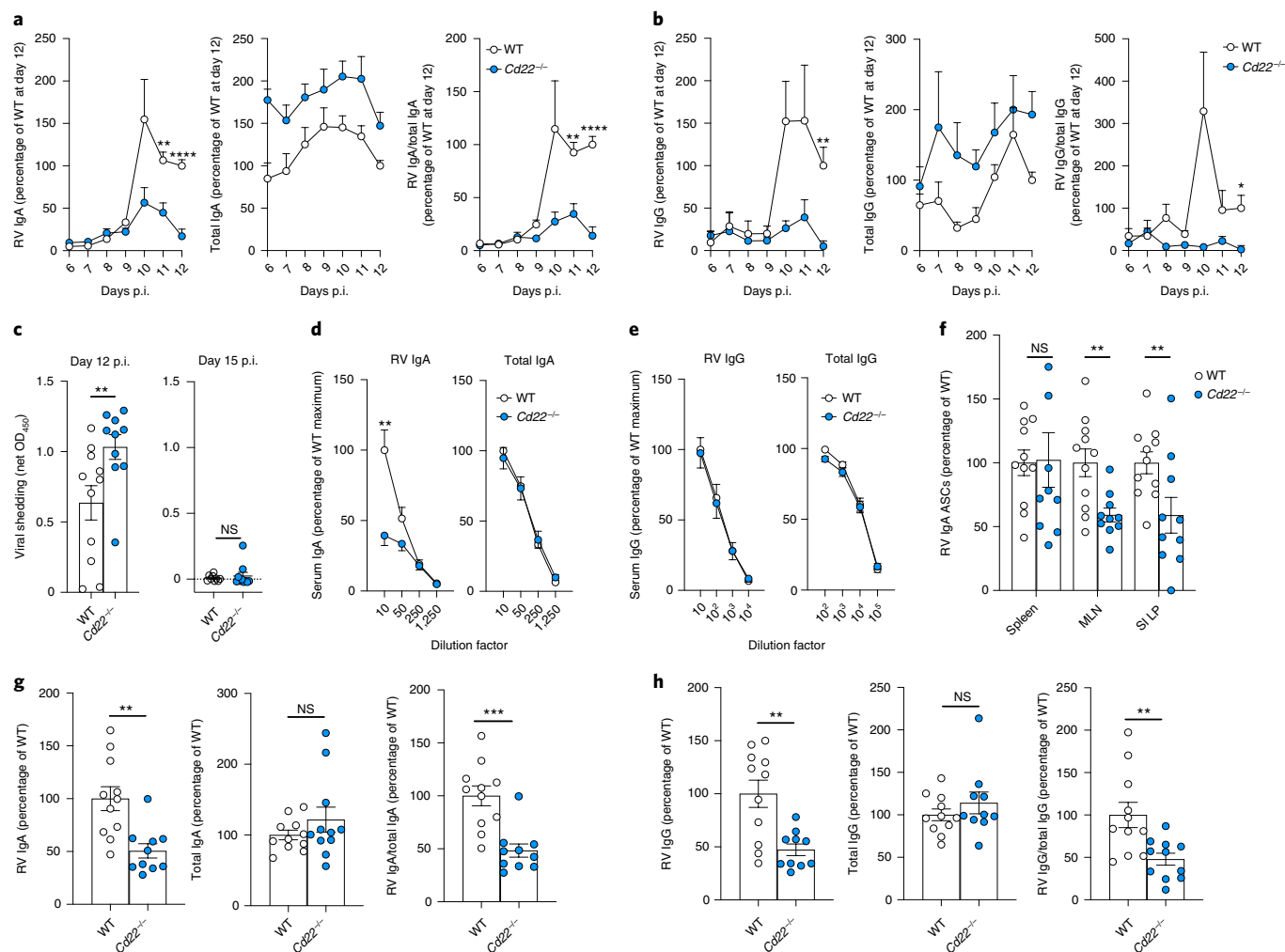
Fig. 8 | Delayed protective immune response to RV infection in CD22-deficient animals. a,b, Five-day-old WT or $Cd22^{-/-}$ pups were orally gavaged with RV strain EW. The production of RV-specific IgA, total IgA and RV IgA normalized to total IgA (**a**) or RV-specific IgG, total IgG and RV IgG normalized to total IgG (**b**) in fecal samples was measured by ELISA up to 12 d post-infection (p.i). The mean of the OD_{450} for the WT group at day 12 post-infection was set to 100 and the data are expressed as a percentage of this total. **c,** Fecal RV antigen shedding, as measured by ELISA and expressed as the net OD_{450}, normalized to the sample weight. In **a–c**, pooled data (means ± s.e.m.) from $n = 4$ independent experiments are shown, with 10–15 animals per group in total. **d–h,** In separate experiments, 5-day-old WT and $Cd22^{-/-}$ pups were orally inoculated with RV strain EW and sacrificed at day 12 post-infection. **d,e,** Serum levels of RV-specific IgA and total IgA (**d**) and RV-specific IgG and total IgG (**e**) as measured by ELISA. The mean of the maximum OD_{450} for the WT group was set to 100 and the data are expressed as a percentage of this total. **f,** Numbers of RV-specific IgA ASCs measured in the spleen, MLN and small intestine lamina propria (SI LP) by ELISPOT. Shown are the numbers of RV IgA ASCs per 10^6 total cells, expressed as a percentage of the WT group mean. **g,h,** Ex vivo small intestine fragment cultures. The data are displayed and presented as in Fig. 7e,f to show RV IgA, total IgA and ratios of RV IgA to total IgA (**g**) and RV IgG, total IgG and ratios of RV IgG to total IgG (**h**), as measured by ELISA. Shown in **d–h** are pooled data (means ± s.e.m.) from $n = 2$ experiments, with 10–11 mice per group in total. Groups were compared by two-way ANOVA with Šidák's multiple comparisons test (**a**, **b**, **d** and **e**) or unpaired two-tailed Student's t-test (**c** and **f–h**). **$P \leq 0.01$; ***$P \leq 0.001$.

by *St6Gal1*. *St6Gal1*$^{-/-}$ PP HEVs are defective at recruiting CD22-expressing B cells in short-term homing assays[48], probably as a result of *trans* interactions between CD22 and α2-6-Sia-decorated glycans on HEVs. Yet, we showed here that even in the absence of HEV CD22 ligands, the reduced $\alpha_4\beta_7$ on $Cd22^{-/-}$ B cells inhibits homing to the PP. In contrast with the effects of a defective CD22–Shp1 axis, which inhibits tethering and speeds up rolling, intravital microscopy in *St6Gal1*$^{-/-}$ mice revealed that wild-type B cells tether and roll normally on *St6Gal1*$^{-/-}$ PP HEVs: only definitive arrest is compromised (unpublished observations). We hypothesize that CD22 ligation to α2-6-Sia-modified MAdCAM-1 creates a synapse between CD22, MAdCAM-1 and $\alpha_4\beta_7$, facilitating chemokine-driven activation of $\alpha_4\beta_7$ and arrest of the B cell. An analogous mechanism controls the arrest of neutrophils:

heterophilic ligation of endothelial-cell-expressed CD99 to paired immunoglobulin-like receptors enhances the chemokine-induced β_2-dependent arrest of neutrophils on intercellular adhesion molecule 1 (ref. [49]). Future studies will probably shed light on this complex mechanism. It is fascinating that CD22 has evolved these two separate functions: (1) selective regulation of surface β_7 expression; and (2) *trans*-ligation to PP HEV heterophilic ligands, to serve the same goal of enhancing B cell homing to the GALT.

Online content
Any methods, additional references, Nature Research reporting summaries, source data, extended data, supplementary information, acknowledgements, peer review information; details of author contributions and competing interests; and statements of

References

1. Berlin, C. et al. α4β7 integrin mediates lymphocyte binding to the mucosal vascular addressin MAdCAM-1. *Cell* **74**, 185–195 (1993).
2. Bargatze, R. F., Jutila, M. A. & Butcher, E. C. Distinct roles of L-selectin and integrins α4β7 and LFA-1 in lymphocyte homing to Peyer's patch-HEV in situ: the multistep model confirmed and refined. *Immunity* **3**, 99–108 (1995).
3. Streeter, P. R., Berg, E. L., Rouse, B. T. N., Bargatze, R. F. & Butcher, E. C. A tissue-specific endothelial cell molecule involved in lymphocyte homing. *Nature* **331**, 41–46 (1988).
4. Butcher, E. C., Williams, M., Youngman, K., Rott, L. & Briskin, M. Lymphocyte trafficking and regional immunity. *Adv. Immunol.* **72**, 209–253 (1999).
5. Stevens, S. K., Weissman, I. L. & Butcher, E. C. Differences in the migration of B and T lymphocytes: organ-selective localization in vivo and the role of lymphocyte–endothelial cell recognition. *J. Immunol.* **128**, 844–851 (1982).
6. Tang, M. L., Steeber, D. A., Zhang, X. Q. & Tedder, T. F. Intrinsic differences in L-selectin expression levels affect T and B lymphocyte subset-specific recirculation pathways. *J. Immunol.* **160**, 5113–5121 (1998).
7. Green, M. C. & Shultz, L. D. *Motheaten*, an immunodeficient mutant of the mouse: I. Genetics and pathology. *J. Hered.* **66**, 250–258 (1975).
8. Coman, D. R. E. X. & Bailey, C. L. "*Viable Motheaten*," a new allele at the *Motheaten* locus. *Am. J. Pathol.* **116**, 179–192 (1984).
9. Neel, B. G., Gu, H. & Pao, L. The 'Shp'ing news: SH2 domain-containing tyrosine phosphatases in cell signaling. *Trends Biochem. Sci.* **28**, 284–293 (2003).
10. Zhang, J., Somani, A. K. & Siminovitch, K. A. Roles of the SHP-1 tyrosine phosphatase in the negative regulation of cell signalling. *Semin. Immunol.* **12**, 361–378 (2000).
11. Sauer, M. G., Herbst, J., Diekmann, U., Rudd, C. E. & Kardinal, C. SHP-1 acts as a key regulator of alloresponses by modulating LFA-1-mediated adhesion in primary murine T cells. *Mol. Cell Biol.* **36**, 3113–3127 (2016).
12. Meyer, S. J., Linder, A. T., Brandl, C. & Nitschke, L. B cell Siglecs—news on signaling and its interplay with ligand binding. *Front. Immunol.* **9**, 2820 (2018).
13. Pao, L. I. et al. B cell-specific deletion of protein-tyrosine phosphatase Shp1 promotes B-1a cell development and causes systemic autoimmunity. *Immunity* **27**, 35–48 (2007).
14. Mercadante, E. R. & Lorenz, U. M. T cells deficient in the tyrosine phosphatase SHP-1 resist suppression by regulatory T cells. *J. Immunol.* **199**, 129–137 (2017).
15. Martinez, R. J., Morris, A. B., Neeld, D. K. & Evavold, B. D. Targeted loss of SHP1 in murine thymocytes dampens TCR signaling late in selection. *Eur. J. Immunol.* **46**, 2103–2110 (2016).
16. Müller, J. et al. CD22 ligand-binding and signaling domains reciprocally regulate B-cell Ca²⁺ signaling. *Proc. Natl Acad. Sci. USA* **110**, 12402–12407 (2013).
17. Han, S., Collins, B. E., Bengtson, P. & Paulson, J. C. Homomultimeric complexes of CD22 in B cells revealed by protein–glycan cross-linking. *Nat. Chem. Biol.* **1**, 93–97 (2005).
18. Stamenkovic, I., Sgroi, D., Aruffo, A., Sy, M. S. & Anderson, T. The B lymphocyte adhesion molecule CD22 interacts with leukocyte common antigen CD45RO on T cells and α2–6 sialyltransferase, CD75, on B cells. *Cell* **66**, 1133–1144 (1991).
19. Gasparrini, F. et al. Nanoscale organization and dynamics of the siglec CD22 cooperate with the cytoskeleton in restraining BCR signalling. *EMBO J.* **35**, 258–280 (2015).
20. Hennet, T., Chui, D., Paulson, J. C. & Marth, J. D. Immune regulation by the ST6Gal sialyltransferase. *Proc. Natl Acad. Sci. USA* **95**, 4504–4509 (1998).
21. Cullen, P. J. & Steinberg, F. To degrade or not to degrade: mechanisms and significance of endocytic recycling. *Nat. Rev. Mol. Cell Biol.* **19**, 679–696 (2018).
22. van Weert, A. W. M., Geuze, H. J., Groothuis, B. & Stoorvogel, W. Primaquine interferes with membrane recycling from endosomes to the plasma membrane through a direct interaction with endosomes which does not involve neutralisation of endosomal pH nor osmotic swelling of endosomes. *Eur. J. Cell Biol.* **79**, 394–399 (2000).
23. Legate, K. R. & Fassler, R. Mechanisms that regulate adaptor binding to β-integrin cytoplasmic tails. *J. Cell Sci.* **122**, 187–198 (2008).
24. Oxley, C. L. et al. An integrin phosphorylation switch: the effect of β3 integrin tail phosphorylation on Dok1 and talin binding. *J. Biol. Chem.* **283**, 5420–5426 (2008).
25. Calderwood, D. A. et al. Integrin β cytoplasmic domain interactions with phosphotyrosine-binding domains: a structural prototype for diversity in integrin signaling. *Proc. Natl Acad. Sci. USA* **100**, 2272–2277 (2003).
26. Smith, M. J., Hardy, W. R., Murphy, J. M., Jones, N. & Pawson, T. Screening for PTB domain binding partners and ligand specificity using proteome-derived NPXY peptide arrays. *Mol. Cell. Biol.* **26**, 8461–8474 (2006).
27. Anthis, N. J. et al. β integrin tyrosine phosphorylation is a conserved mechanism for regulating talin-induced integrin activation. *J. Biol. Chem.* **284**, 36700–36710 (2009).
28. Caswell, P. T., Vadrevu, S. & Norman, J. C. Integrins: masters and slaves of endocytic transport. *Nat. Rev. Mol. Cell Biol.* **10**, 843–853 (2009).
29. Butcher, E. C., Szabo, M. C. & McEvoy, L. M. Specialization of mucosal follicular dendritic cells revealed by mucosal addressin-cell adhesion molecule-1 display. *J. Immunol.* **158**, 5584–5588 (1997).
30. Altevogt, P. et al. The α4 integrin chain is a ligand for α4β7 and α4β1. *J. Exp. Med.* **182**, 345–355 (1995).
31. Williams, M. B. et al. The memory B cell subset responsible for the secretory IgA response and protective humoral immunity to rotavirus expresses the intestinal homing receptor, α4β7. *J. Immunol.* **161**, 4227–4235 (1998).
32. Habtezion, A., Nguyen, L. P., Hadeiba, H. & Butcher, E. C. Leukocyte trafficking to the small intestine and colon. *Gastroenterology* **150**, 340–354 (2016).
33. Seong, Y. et al. Trafficking receptor signatures define blood plasmablasts responding to tissue-specific immune challenge. *JCI Insight* **2**, e90233 (2017).
34. Franco, M. A. & Greenberg, H. B. Immunity to rotavirus infection in mice. *J. Infect. Dis.* **179**, 466–469 (1999).
35. Anthis, N. J. et al. β integrin tyrosine phosphorylation is a conserved mechanism for regulating talin-induced integrin activation. *J. Biol. Chem.* **284**, 36700–36710 (2009).
36. Tehran, D. A., López-Hernández, T. & Maritzen, T. Endocytic adaptor proteins in health and disease: lessons from model organisms and human mutations. *Cells* **8**, 1345 (2019).
37. Nishimura, T. & Kaibuchi, K. Numb controls integrin endocytosis for directional cell migration with aPKC and PAR-3. *Dev. Cell* **13**, 15–28 (2007).
38. Sun, H. et al. Distinct chemokine signaling regulates integrin ligand specificity to dictate tissue-specific lymphocyte homing. *Dev. Cell* **30**, 61–70 (2014).
39. Steinberg, F., Heesom, K. J., Bass, M. D. & Cullen, P. J. SNX17 protects integrins from degradation by sorting between lysosomal and recycling pathways. *J. Cell Biol.* **197**, 219–230 (2012).
40. Ghai, R. et al. Structural basis for endosomal trafficking of diverse transmembrane cargos by PX-FERM proteins. *Proc. Natl Acad. Sci. USA* **110**, 643–652 (2013).
41. Nitschke, L., Carsetti, R., Ocker, B., Köhler, G. & Lamers, M. C. CD22 is a negative regulator of B-cell receptor signalling. *Curr. Biol.* **7**, 133–143 (1997).
42. Schippers, A. et al. β7 integrin controls immunogenic and tolerogenic mucosal B cell responses. *Clin. Immunol.* **144**, 87–97 (2012).
43. Sato, S. et al. CD22 is both a positive and negative regulator of B lymphocyte antigen receptor signal transduction: altered signaling in CD22-deficient mice. *Immunity* **5**, 551–562 (1996).
44. Feng, N., Franco, M. A. & Greenberg, H. B. in *Mechanisms in the Pathogenesis of Enteric Diseases* (eds Paul, P. S. et al.) 233–240 (Springer, 1997).
45. Marcelin, G., Miller, A. D., Blutt, S. E. & Conner, M. E. Immune mediators of rotavirus antigenemia clearance in mice. *J. Virol.* **85**, 7937–7941 (2011).
46. Blutt, S. E., Miller, A. D., Salmon, S. L., Metzger, D. W. & Conner, M. E. IgA is important for clearance and critical for protection from rotavirus infection. *Mucosal Immunol.* **5**, 712–719 (2012).
47. Lopatin, U., Blutt, S. E., Conner, M. E. & Kelsall, B. L. Lymphotoxin alpha-deficient mice clear persistent rotavirus infection after local generation of mucosal IgA. *J. Virol.* **87**, 524–530 (2012).
48. Lee, M. et al. Transcriptional programs of lymphoid tissue capillary and high endothelium reveal control mechanisms for lymphocyte homing. *Nat. Immunol.* **15**, 982–995 (2014).
49. Goswami, D. et al. Endothelial CD99 supports arrest of mouse neutrophils in venules and binds to neutrophil PILRs. *Blood* **129**, 1811–1822 (2017).

Methods

Reagents. All of the antibodies used in these studies are listed in Supplementary Table 1 and the Nature Research Reporting Summary linked to this article.

Mice. C57BL/6 WT, BALB/c WT, $Cd22^{-/-}$ (ref. [41]) and $St6gal1^{-/-}$ mice[20] were bred and housed in the animal facilities of the Veterans Affairs Palo Alto Health Care System, accredited by the Association for Assessment and Accreditation of Laboratory Animal Care. CD22^{Y2,5,6F} (ref. [16]) and CD22^{R130E} mice[16] were bred and housed at the Department of Biology of the University of Erlangen. $Ptpn6^{meV/meV}$ and $Ptpn6^{+/meV}$ mice[8] were bred and housed at the University of California, San Francisco. All animals were housed under standard conditions, maintained in a 12 h/12 h light/dark cycle at $22 \pm 2\,^{\circ}C$ and given food and tap water ad libitum. Unless otherwise stated, 6- to 12-week-old male and female mice were used in all of the experiments. All animal work and housing conditions were approved by the Institutional Animal Care and Use Committee at the Veterans Affairs Palo Alto Health Care System, or by the relevant animal care committees at the University of Erlangen.

Integrin expression and lymphocyte cellularity by flow cytometry. Lymphocytes from the blood, PLNs (inguinal, axillary and brachial lymph nodes), MLNs, bone marrow and PPs (average of five PPs per mouse) of WT and mutant mice were isolated and stained with fluorescently labeled antibodies against CD4, CD3ε, CD19, IgD and either $α_L$, $β_2$, $α_4$, $β_1$, $β_7$, $α_4β_7$ or the appropriate isotype control. The Fc receptors were blocked using rat serum and anti-CD16/32 before staining. Dead cells were excluded by staining with 4′,6-diamidino-2-phenylindole (DAPI) or the LIVE/DEAD Fixable Aqua dye (Invitrogen). For the integrin expression studies, the MFI of the isotype control was subtracted from the MFI of the integrin staining. The integrin staining MFI (background corrected) was expressed as a percentage of the WT C57BL/6 (control group) mean MFI. For the cellularity studies, we added CountBright counting beads (Invitrogen) to each sample to calculate the absolute cell number per organ. Samples were acquired on a Fortessa flow cytometer (BD Biosciences) using FACSDiva Software (BD Biosciences; version 8.0.1), and were analyzed using FlowJo (BD Biosciences; 10.3). A representative gating strategy is shown in Supplementary Fig. 1.

In situ video microscopy analyses of lymphocyte interactions with PP HEVs. Naive B cells or CD4$^+$ T cells were isolated from WT and $Cd22^{-/-}$ or $Ptpn6^{+/meV}$ splenocytes using negative selection kits (STEMCELL Technologies). For each experiment, the quality of the isolation was checked by flow cytometry and consisted of ≥98% cells of interest. Lymphocytes were labeled with 2.5 µM CMFDA (Invitrogen) or CMTPX dye (Invitrogen) for 10 min at 37 °C in RPMI without fetal bovine serum (FBS), then washed with RPMI containing 10% FBS. In some experiments, labeled B or CD4$^+$ T cells were incubated with the anti-mouse $α_4β_7$ antibody DATK32 (50 µg ml^{-1})[50] in RPMI containing 10% FBS for 45 min at 37 °C. Cells were washed three times to remove unbound antibodies. Before injection into recipient mice, cells were counted by flow cytometry using counting beads. Recipient mice were anesthetized via intraperitoneal injection of ketamine and xylazine. One individual PP of the small intestine was exteriorized and positioned for epifluorescence microscopy and video recording. The same numbers (5–10 × 10^6 cells) of WT, $Cd22^{-/-}$, $Ptpn6^{+/meV}$ B or CD4$^+$ T cells were transferred into anesthetized recipients. The interactions of fluorescent cells with PP HEVs were recorded for 30–40 s at 40 frames per second of 25 ms exposure time. All fluorescent cells entering HEVs during the recording time were analyzed on a frame-to-frame basis for the entire duration of the video. Cells passing HEVs for <1 s with no interaction, or with a velocity >300 µm s^{-1}, were considered non-interactive and called flyers. Cells that started binding to HEVs briefly for <1 s before getting released were considered non-interactive and called brief rollers. Cells binding to HEVs for >1 s were considered rollers. At the end of the recording, rollers attached to HEVs with a static binding of >2 s were considered arresters. To assess the mean rolling velocity of each cell, we tracked each cell manually using Imaris (version 9) to define the precise rolling distance from the frame of its first interaction (f_{first}) to the first frame of its definitive static binding (f_{last}). The rolling time was $(f_{last} - f_{first} + 1) \times 25$ ms.

Short-term homing assay. Donor splenocytes were isolated and labeled with CellTrace Violet (Invitrogen) or CFSE (Invitrogen) in complete RPMI medium, or a combination of CellTrace Violet and CFSE at concentrations optimized for a bar-coding system with two to four donor populations in total. Equal numbers (25–50 × 10^6 cells) of donor cells were transferred into WT recipient mice by injection into the tail vein. After 1.5 h, lymphocytes from the PLNs and PPs (average of five PPs per mouse) of recipient mice were isolated and stained for flow cytometry to identify T and B cells (see 'Integrin expression and lymphocyte cellularity by flow cytometry'). The LIVE/DEAD Fixable Aqua dye was used for live/dead staining, and counting beads were added to calculate absolute cell numbers. The efficiency of B and T cell homing to each organ was calculated as a ratio: the number of cells found in each organ was divided by the number of cells injected (input). Then, the results were presented as a percentage of the WT C57BL/6 (control group) mean ratio.

PLA. B cells were isolated from WT and $Cd22^{-/-}$ splenocytes using negative selection kits. In some experiments, B cells were pre-treated with *Arthrobacter uereafaciens* sialidase (Roche) at 125 mU ml^{-1} to remove α2-6-Sia modifications. Vehicle-control-treated (phosphate-buffered saline (PBS)) or sialidase-treated purified B cells were cytospun on to a 1 cm^2 area of a slide at a concentration of 1.5×10^5 per 100 µl for 7 min at 700 r.p.m. in a Cyto-Tek centrifuge (model number 4324). The cell sections were fixed using 4% paraformaldehyde for 5 min at 4 °C, followed by washing with PBS three times. All subsequent incubations were carried out in a humidity chamber at 37 °C following the Duolink PLA kit (Sigma–Aldrich) instructions. The following combinations of primary antibodies were used: mouse anti-mouse CD22 (Cy34.1) and goat anti-mouse $β_7$ or goat anti-mouse $β_1$; and goat anti-mouse $β_1$ and rat anti-mouse $α_4$ (PS/2) followed by In Situ PLA Probe Anti-Mouse MINUS and Anti-Goat PLUS (Sigma–Aldrich). At the end of the PLA procedure, the sections were stained with DAPI for the identification of nuclei. Images were captured on a Zeiss LSM 880 confocal microscope using the Zeiss ZEN software, a 63× oil-immersion objective and a 1.5× digital zoom. The number of PLA spots per image were quantified using Imaris (version 2.0.0-rc-49/1.51d).

Cellular localization of integrin β7, CD22 and Shp1 by microscopy. B cells were isolated from WT and $Cd22^{-/-}$ splenocytes using negative selection kits. In some experiments, cells were stained with MitoTracker Deep Red FM (Invitrogen) at 0.5 µM for 15 min at 37 °C to identify the cytoplasm. Cells were fixed using 1% paraformaldehyde (Invitrogen) in PBS for 5 min at 4 °C, then stained for extracellular $β_7$ and CD22 with goat anti-mouse $β_7$ and biotin mouse anti-mouse CD22, respectively, in PBS for 40 min at 4 °C, followed by Alexa Fluor 488-conjugated donkey anti-goat (for $β_7$) and Alexa Fluor 594-conjugated streptavidin (for CD22) for 40 min at 4 °C. In some experiments, cells were permeabilized in 1× permeabilization buffer from Invitrogen for 30 min at 4 °C after fixation, stained for Shp1, $β_7$ and CD22 with rabbit anti-human/mouse Shp1, goat anti-mouse $β_7$ and biotin mouse anti-mouse CD22, respectively, in 1× permeabilization buffer for 60 min at 4 °C, washed with fresh 1× permeabilization buffer, then stained with Alexa Fluor 594-conjugated donkey anti-rabbit (for Shp1), Alexa Fluor 488 donkey anti-goat (for $β_7$) and Alexa Fluor 647-conjugated streptavidin (for CD22). At the end of the staining procedure, cells were cytospun and stained with DAPI for the identification of nuclei, and images were captured as described above (see 'PLA'). For each cell, we quantified the intensity of the $β_7$ fluorescence with ImageJ using the corrected total cell fluorescence. We counted manually the total number of $β_7$ spots at the cell surface found in close proximity with intracellular spots of Shp1 and expressed this number as a percentage of the total $β_7$ spots to yield a Shp1–$β_7$ proximity index (%). Similarly, we counted the total number of CD22 spots at the cell surface found in close proximity to both $β_7$ and Shp1 and expressed this number as a percentage of the total $β_7$/Shp1 hotspots to yield a CD22–Shp1/$β_7$ proximity index (%).

Endocytosis assay. Splenocytes were stained with fluorescently labeled antibodies against CD19, IgD and either CD71 TfR1, $β_1$, $β_7$ or the appropriate isotype control. The Fc receptors were blocked with anti-CD16/32 before the staining. For each sample, staining at 4 °C with phycoerythrin-conjugated RI7217 (anti-TfR1), HMβ1-1 (anti-$β_1$), FIB504 (anti-$β_7$) or the matching phycoerythrin-conjugated isotype control antibodies allowed calculation for extracellular amounts of TfR1, $β_1$, $α_L$ and $β_7$ concentrations. We used pHrodo iFL microscale protein labeling kits (Invitrogen) to label the antibody clones HMβ1-1, FIB504 or isotype-matched controls. In parallel, staining of each sample with pHrodo Red-conjugated transferrin (Invitrogen), HMβ1-1, FIB504 or isotype control antibodies at either 4 °C (no endocytosis) or 37 °C (endocytosis) for 1 h was used to calculate the endocytosis efficiency. The same staining protocol was performed in the presence of 100 µM primaquine. Samples were analyzed by flow cytometry. For each antigen and each experiment, the RER was calculated by normalizing endocytosis levels to extracellular levels as follows:

$$\text{RER (of antigen A)} = \frac{\text{MFI of anti}-\text{A pHrodo Red staining at 37 }^{\circ}C}{\text{MFI of anti}-\text{A phycoerythrin staining at 4 }^{\circ}C} - \frac{\text{MFI of anti}-\text{A pHrodo Red staining at 4 }^{\circ}C}{\text{MFI of isotype control phycoerythrin staining at 4 }^{\circ}C}$$

Double immunoprecipitation and immunoblotting. Purified B or T cells were labeled with EZ-Link Sulfo-NHS-Biotin (Invitrogen) on ice for 60 min. Biotinylated cells were washed with Hanks' balanced salt solution and lysed in immunoprecipitation buffer (50 mM Tris-HCl (pH 7.5; Sigma–Aldrich), 150 mM NaCl (Sigma–Aldrich), 1% Triton X-100 (Sigma–Aldrich), 0.1% sodium deoxycholate (Sigma–Aldrich), 1 mM EDTA (Invitrogen), cOmplete, Mini, EDTA-free Protease Inhibitor (Roche) and Phosphatase Inhibitor Cocktail 2 and 3 (Sigma–Aldrich) used at 1:100 dilution from stock) for 20 min on ice. Cell lysates were cleared from debris by centrifugation (16,000g; 10 min; 4 °C). After pre-clearing the lysates with unbound Dynabeads protein G beads (Invitrogen), $β_7$ integrin was pulled down by incubation of lysates with Dynabeads protein G bound to rat anti-mouse $β_7$ antibody FIB504 (ref. [51]) at 4 °C overnight with

agitation. After several washes with immunoprecipitation buffer, the β_7 integrin was eluted with 100 mM glycine buffer at pH 2.5 for 15 min at 56 °C with gentle agitation. The acidic pH of the eluate was then quenched with two volumes of 100 mM Tris-HCl (pH 8.0). Biotinylated β_7 was pulled down from these eluates with SoftLink Soft Release Avidin Resin (Promega) overnight at 4 °C with agitation. The flowthrough of the streptavidin immunoprecipitation was spun in with 30 kDa molecular weight cut-off ultrafiltration tubes to concentrate the biotin-free β_7 fraction, then reduced at 95 °C for 5 min with 1× Laemmli buffer (Bio-Rad) containing 5% β-mercaptoethanol (Sigma–Aldrich). After overnight incubation, the avidin resin was washed three times with Tris-buffered saline (Sigma–Aldrich) containing 0.01% Tween 20 (Sigma–Aldrich), and biotinylated β_7 was eluted with 1× Laemmli buffer containing 5% β-mercaptoethanol (95 °C; 5 min). Reduced biotin-free and biotinylated β_7 were then subjected to sodium dodecyl sulfate polyacrylamide gel electrophoresis and immunoblot analysis. Integrin β_7 was detected from immunoblots with rat anti-mouse β_7 antibody (clone FIB504) plus horseradish peroxidase-conjugated goat anti-rat antibodies, followed by the addition of enhanced chemiluminescence substrate (Clarity Western ECL Substrate; Bio-Rad). Blots were stripped (Restore PLUS Western Blot Stripping Buffer; Invitrogen) and tyrosine phosphorylation was detected with the mouse anti-p-Tyr antibody (clone PY20) plus horseradish peroxidase-conjugated goat anti-mouse followed by addition of the substrate. Images were captured using the Azure Biosystems 600 imaging system. Imaged blots were quantified using ImageJ.

Real-time quantitative PCR with reverse transcription (RT-qPCR). Total RNA was isolated from purified B cells using the RNeasy Mini Kit (Qiagen). Analysis of total RNA concentration and integrity was assessed using NanoDrop ND-1000 spectrophotometry. Equal amounts of each total RNA sample were converted into complementary DNA (cDNA) using the High-Capacity cDNA Reverse Transcription Kit (Invitrogen) according to the manufacturer's instructions. RT-qPCR analysis of genes of interest was performed using SYBR Green on an ABI PRISM 7900HT (Applied Biosystems). PCR reaction mixtures consisted of 1 µl of a 1:5 dilution of template cDNA, 200 nM of each primer and 1× Power SYBR Green PCR Master Mix (Invitrogen) in a final volume of 10 µl. RT-qPCR amplication was conducted using an initial step of 5 min at 45 °C, then 5 min at 95 °C, followed by 40 cycles of denaturation at 95 °C for 30 s, primer annealing at 60 °C for 30 s and extension at 72 °C for 30 s. Melting curve analysis was used to assess the purity of the amplified bands. The sequences for the primer pairs used for *Itgal*[52] (ref. [52]), *Itgb1* (ref. [52]), *Itgb2* (ref. [52]), *Itgb7*[53] (ref. [53]) and *Hprt*[54] are listed in Supplementary Table 2. Primer pairs for *Actb* were pre-designed from Qiagen. We used the $2^{-\Delta\Delta Ct}$ method to calculate the relative gene mRNA expression of *Itgal*, *Itgb1*, *Itgb2* and *Itgb7* using *Actb* and *Hprt* as housekeeping genes.

CTB immunization studies. Adult C57BL/6 or *Cd22*$^{-/-}$ mice were immunized with 10 µg CTB (Sigma–Aldrich) diluted in 100 µl PBS for oral gavage (oral route), 10 µl PBS for intranasal administration via pipetting in the nostrils (nasal route) or 50 µl PBS for injection into the mouse hamstring (muscular route). Mice were sacrificed 2 weeks after the immunizations. Serum was collected for enzyme-linked immunosorbent assay (ELISA) studies, and segments of small intestine were used in ex vivo cultures.

RV infection studies. Five-day-old C57BL/6 or *Cd22*$^{-/-}$ pups were orally gavaged with 10^4 DD50 (that is, diarrhea dose 50%, the highest dilution of a virus stock that caused diarrhea in 50% of suckling mice) of WT murine RV (strain EW) diluted in M199 medium. Pups were then checked daily for diarrhea by gentle abdominal pressure. Fecal samples from each individual mouse were collected in PBS with calcium/magnesium for ELISAs. In some studies, mice were sacrificed at day 12 post-infection to collect serum for ELISA studies; MLNs, small intestine lamina propria and spleen for enzyme-linked immune absorbent spot (ELISPOT) analysis; and segments of small intestine for ex vivo cultures.

Detection of viral antigen and virus-specific IgA and IgG by ELISA. For the detection of viral antigen in fecal samples[55], 96-well ELISA plates were coated with guinea pig anti-RV hyperimmune serum in PBS and incubated at 37 °C for 4 h. The plates were then blocked with 5% non-fat milk in PBS (Blotto) at 37 °C for 2 h. Suspended fecal samples were diluted 1:20 in 1% Blotto, added to the plates and incubated at 37 °C for 1 h. The plates were washed three times with PBS containing 0.05% Tween 20 (PBS-T). Rabbit anti-RV hyperimmune serum in 1% Blotto was added to the plates for 1 h at 37 °C and washed three times. Horseradish peroxidase-conjugated goat anti-rabbit IgG in 1% Blotto was added to the plates and incubated for 1 h at 37 °C. TMB substrate (Sigma–Aldrich) was added after four washes in PBS-T, the plates were developed for 10 min at room temperature, the reaction was stopped by the addition of 0.16 M sulfuric acid, and the optical density measured at a wavelength of 450 nm (OD$_{450}$) was read with a plate reader. The data are presented as OD$_{450}$-like numbers after normalization to stool weight.

For the detection of virus-specific fecal and serum IgA and IgG, plates were coated with rabbit anti-RV hyperimmune serum and blocked as described above, then incubated with 1:5 of RV stock (a gift from H. Greenberg at Stanford University) in 1% Blotto overnight at 4 °C. After three washes with PBS-T, stool samples (1:20 in Blotto) or serial dilutions of serum in 1% Blotto were added to the

plates. After 2 h incubation at 37 °C, the plates were washed three times in PBS-T and peroxidase-conjugated anti-mouse IgA or IgG was added for 1 h at 37 °C. The plates were washed and developed as described above. For the detection of total fecal and serum IgA or IgG, the plates were coated with anti-mouse IgA, IgG or IgM polyclonal antibodies before using the same protocol as above.

Detection of CTB-specific IgA and IgG by ELISA. ELISA plates were coated with CTB (2 µg ml^{-1}) overnight, blocked with PBS containing 5% bovine serum albumin (BSA), then incubated with serial dilutions of serum or ex vivo small intestine culture samples diluted in PBS containing 2% BSA for 2 h. After four washes with PBS-T, peroxidase-conjugated anti-mouse IgA or IgG in 2% BSA was added for 1 h at 37 °C. TMB substrate was added after four washes in PBS-T, the plates were developed for 5–10 min at room temperature, the reaction was stopped by the addition of 0.16 M sulfuric acid and the OD$_{450}$ was read with a plate reader. For the detection of total IgA or IgG in serum and ex vivo small intestine culture samples, plates were coated with anti-mouse IgA, IgG or IgM polyclonal antibodies before using the same protocol as described above.

Small intestine fragment cultures. Open segments (1 cm long) of duodenums were weighted and placed in 24-well plates on an elevated mesh filter and cultured for 3 days at 37 °C in complete RPMI medium under hyper-oxygenated conditions[56]. At the end of the incubation period, intestinal IgA and IgG were measured by ELISA in the supernatants, as described above.

Quantitation of virus-specific antibody-secreting cells (ASCs) by ELISPOT assay. Multiscreen 96-well plates (MAIPS4510; Millipore) were coated with purified RV double-layer particles (a gift from H. Greenberg (Stanford University)) overnight at 4 °C, washed and blocked with RPMI medium containing 10% fetal calf serum for 1 h at 37 °C. Serial tenfold dilutions of spleen, PP or small intestine lamina propria cells were added to the plates and incubated overnight at 37 °C. After six washes, peroxidase-conjugated anti-mouse IgA or IgG was added for 1 h at 37 °C. The plates were washed six times and developed with AEC substrate (Vector Laboratories). To quantity non-specific ASCs, the plates were coated with anti-mouse IgA, IgG or IgM polyclonal antibodies before using the same protocol as above.

Statistical analyses. All data were organized in Microsoft Excel (version 16.42) spreadsheets and we performed all of our statistical analyses using GraphPad Prism (version 8.4.1). For each dataset shown and analyzed, the test used is indicated in the figure caption. Statistical significance is indicated by $*P \leq 0.05$, $**P \leq 0.01$, $***P \leq 0.001$ and $****P \leq 0.0001$.

Reporting Summary. Further information on research design is available in the Nature Research Reporting Summary linked to this article.

Data availability

The data that support the findings of this study are available from the corresponding author upon request. Source data are provided with this paper.

References

50. Hamann, A., Andrew, D. P., Jablonski-Westrich, D., Holzmann, B. & Butcher, E. C. Role of alpha 4-integrins in lymphocyte homing to mucosal tissues in vivo. *J. Immunol.* **152**, 3282–3293 (1994).
51. Andrew, D. P. et al. Distinct but overlapping epitopes are involved in alpha 4 beta 7-mediated adhesion to vascular cell adhesion molecule-1, mucosal addressin-1, fibronectin, and lymphocyte aggregation. *J. Immunol.* **153**, 3847–3861 (1994).
52. DeNucci, C. C., Pagán, A. J., Mitchell, J. S. & Shimizu, Y. Control of $\alpha_4\beta_7$ integrin expression and CD4 T cell homing by the β_1 integrin subunit. *J. Immunol.* **184**, 2458–2467 (2010).
53. Eun, J. P. et al. Aberrant activation of integrin $\alpha_4\beta_7$ suppresses lymphocyte migration to the gut. *J. Clin. Invest.* **117**, 2526–2538 (2007).
54. Ocón, B. et al. The glucocorticoid budesonide has protective and deleterious effects in experimental colitis in mice. *Biochem. Pharmacol.* **116**, 73–88 (2016).
55. Franco, M. A. & Greenberg, H. B. Role of B cells and cytotoxic T lymphocytes in clearance of and immunity to rotavirus infection in mice. *J. Virol.* **69**, 7800–7806 (1995).
56. Feng, N. et al. Redundant role of chemokines CCL25/TECK and CCL28/MEC in IgA$^+$ plasmablast recruitment to the intestinal lamina propria after rotavirus infection. *J. Immunol.* **176**, 5749–5759 (2006).

Author contributions

Competing interests

The authors declare no competing interests.

Additional information

Extended data is available for this paper at https://doi.org/10.1038/s41590-021-00862-z.

Supplementary information The online version contains supplementary material available at https://doi.org/10.1038/s41590-021-00862-z.

Correspondence and requests for materials should be addressed to R.B. or E.C.B.

Reprints and permissions information is available at www.nature.com/reprints.

Peer reviewer information *Nature Immunology* thanks Dietmar Vestweber and the other, anonymous, reviewer(s) for their contribution to the peer review of this work. L. A. Dempsey was the primary editor on this article and managed its editorial process and peer review in collaboration with the rest of the editorial team.
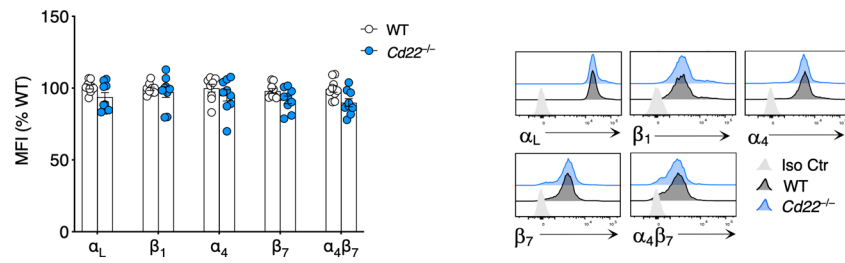
Extended Data Fig. 1 | CD22-deficient T cells display normal cell surface levels of $\alpha_4\beta_7$. Flow cytometry of WT or $Cd22^{-/-}$ live CD3+ CD4+ T cells isolated from spleens and stained with antibodies against the integrins α_L, β_1, α_4, β_7, or $\alpha_4\beta_7$. Shown are pooled data (mean ± SEM) from n = 3 independent experiments with 7 animals per group total presented as in Fig. 1. Representative histogram overlays gated in CD4+ T cells are shown.
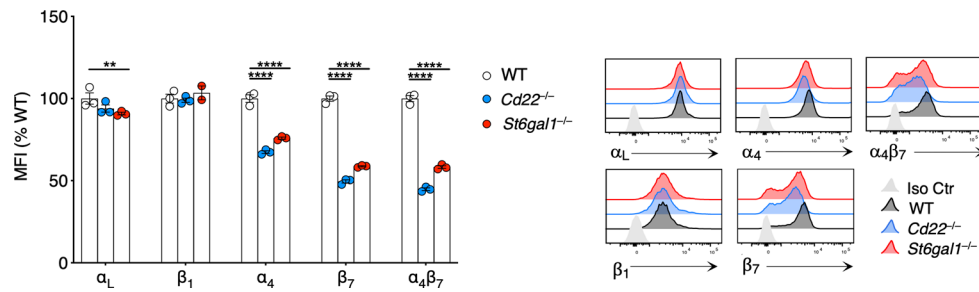
Extended Data Fig. 2 | B cell expression of St6gal1-dependent CD22-binding carbohydrates controls $\alpha_4\beta_7$ expression. Flow cytometry of WT, $Cd22^{-/-}$, or $St6Gal1^{-/-}$ naïve B cell (CD19$^+$ IgD$^+$) isolated from spleen and stained with antibodies against the integrins α_L, β_1, α_4, β_7, or $\alpha_4\beta_7$. Data represent the mean $\pm$ SEM of one representative experiment with n = 3 mice per group presented as in Fig. 1. Representative histogram overlays gated in naïve B cells are shown. Groups were compared using One-way ANOVA with Dunnett's multiple comparisons test. **P $\leq$ 0.01, and ****P $\leq$ 0.0001.
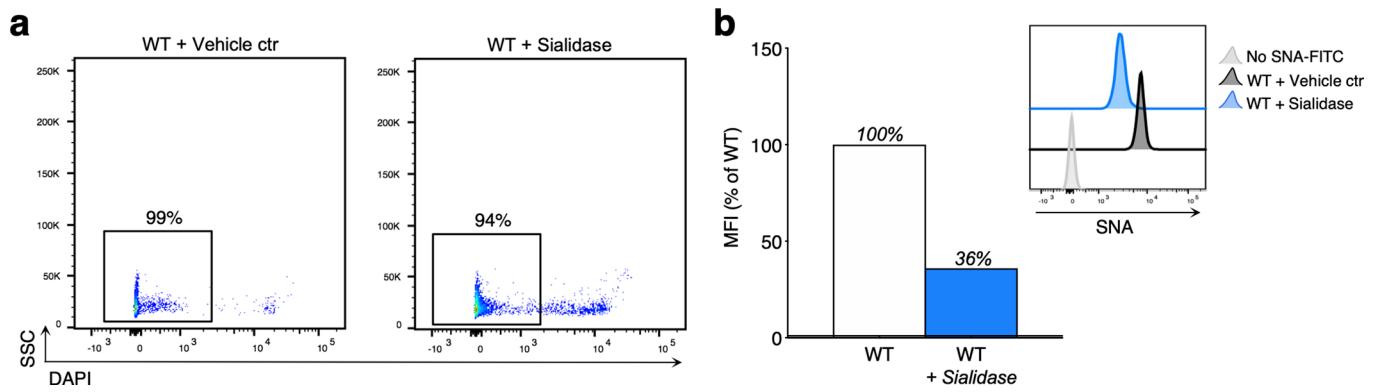
Extended Data Fig. 3 | Removal of α2-6 Sia linkages on B cells with Arthrobacter Uereafaciens sialidase. Purified wild type B cells purified from spleen were incubated for one hour at 37 °C with *Arthrobacter ureafaciens* sialidase or with vehicle control (PBS, Vehicle Ctr). **a,b,** Flow cytometry of *Arthrobacter ureafaciens-treated* or vehicle control-treated WT naïve B cells (CD19+ IgD+), isolated from spleen and stained for DAPI and SNA-FITC. **a**, The percentage of viable cells is shown. **b**, The MFI of the SNA staining was expressed as a percentage of the mean MFI of the vehicle ctr-treated WT B cell group. Representative histogram overlay gated in live naïve B cells is shown.

Extended Data Fig. 4 | CD22-deficient T cells display wild-type levels of tyrosine phosphorylation in cell surface β_7. Left panel: detection of β_7 and phosphotyrosine (pTyr) levels in the cell surface and intracellular β_7 fractions of wild-type (WT) and CD22-deficient ($Cd22^{-/-}$) T cells after the double IP as shown in Fig. 5a. Right panel: quantification of pTyr levels normalized to β_7 levels (pTyr/β_7 ratio). Within each experiment, the pTyr/β_7 of the cell surface β_7 of the WT group was set to 100, and data expressed as a percentage of this total. Each dot represents one independent experiment with n = 4 animals pooled for WT and $Cd22^{-/-}$ (that is n = 8 animals total for the two experimental replicates).
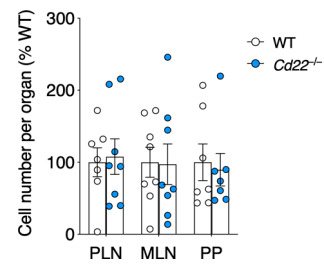
Extended Data Fig. 5 | Normal T cell numbers in CD22-deficient Peyer's patches and lymph nodes. Numbers of CD4+ T cells (CD3+ CD4+) in MLN, PLN, and PP of WT and *Cd22*−/− shown as a percentage of the mean of the WT group. Shown are pooled data (mean ± SEM) of n = 2 experiments with n = 7-8 mice per group total.
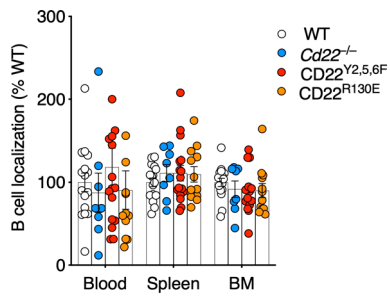
Extended Data Fig. 6 | Functional assays reveal normal homing of CD22 mutant B cells to the spleen and bone marrow. Localization of WT, $Cd22^{-/-}$, CD22^{Y2,5,6F}, and CD22^{R130E} B cells in blood, spleen and bone marrow (BM) after homing assays as illustrated in Fig. 6c. Data are shown as a percentage of the mean localization ratio of the WT group. Shown are pooled data (mean $\pm$ SEM) of n = 3-5 experiments with 11-16 mice per group total.
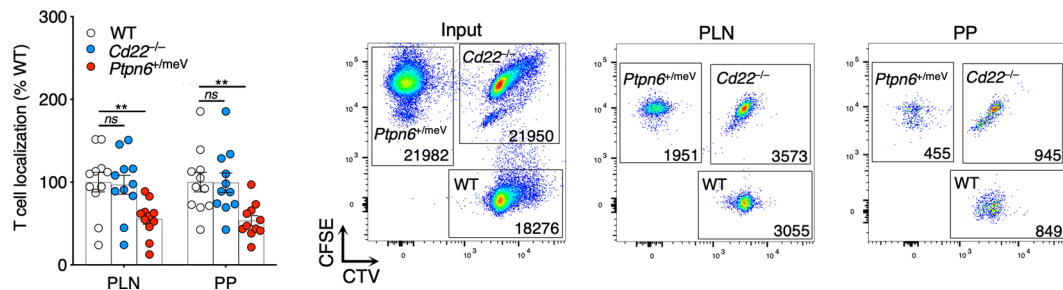
Extended Data Fig. 7 | Localization of WT, *Cd22*$^{-/-}$, and *Ptpn6*$^{+/meV}$ T cells in PLN and PP after short-term homing assays. WT, *Cd22*$^{-/-}$, or *Ptpn6*$^{+/meV}$ splenocytes labeled with CFSE, or CellTracker Violet (CTV) or both were injected i.v. into a recipient WT mouse. PLN, MLN or PP cells isolated from the recipient were stained with anti-CD3 and anti-CD4 for quantification of short-term (90 min) homing of CD4 T cells. For each donor and each organ, the number of isolated CD4 T cells (Output) was normalized to the number of injected CD4 T cells (Input) to yield a T cell localization ratio. Shown is the mean ± SEM from three independent experiments with n = 11 mice per group total. Representative dot plots gated in live CD3$^+$ CD4$^+$ T cells are shown, including the number of cells within each gate. Groups were compared using One-way ANOVA with Dunnett's multiple comparison test. **P ≤ 0.01, and ns: not significant.
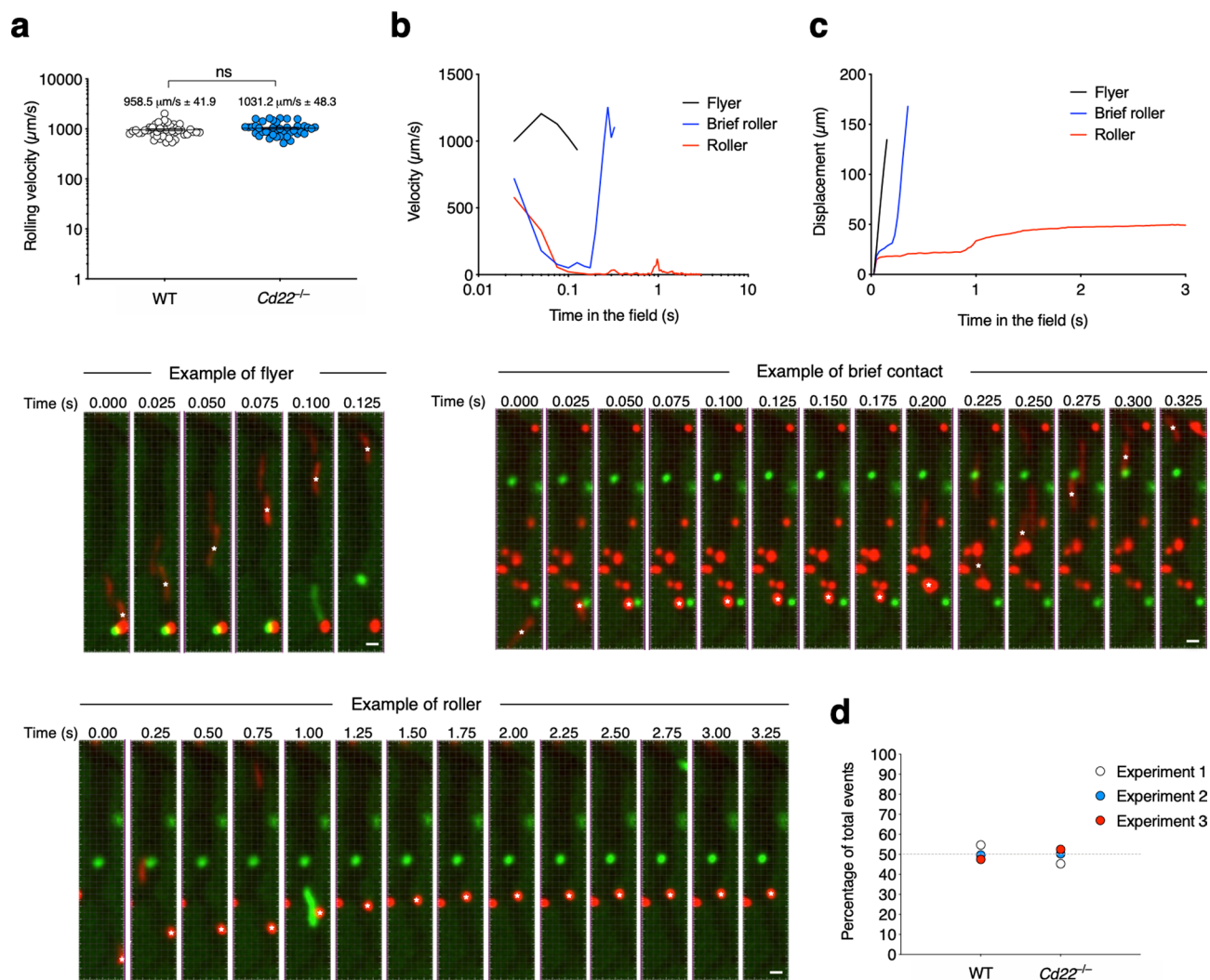
Extended Data Fig. 8 | Definition of flyer, brief roller and roller cells visualized by in situ video microscopy of Peyer's patches. a, The mean velocity of wild-type (WT) and CD22-deficient (*Cd22*⁻/⁻) B cells free flowing through the vessels without any interactions (namely flyer) was calculated and shown for each individual cell. Shown are pooled results (~ 50 cells per group) analyzed from 3–4 representative HEVs and 3 independent experiments. **b,c**, The instant velocity (**b**) and displacement (**c**) of a representative free flowing cell (Flyer), of one that interacts very briefly (<1s) with the HEVs (namely Brief roller), or one that interacts and rolls on the HEVs for >1sec (namely Roller) is shown together with frame-per-frame tracking of the cells (identified with *). Scale bars: 10 μm. **d**, In three independent *in situ* experiments with 1:1 ratio of WT B cells donor versus *Cd22*⁻/⁻ B cells donor, the total number of events (that is flyer, brief roller, or roller) was counted for each donor in 3–4 representative HEVs for the total duration of the movie (~ 250–300 total cells analyzed per group). The percentage of WT and *Cd22*⁻/⁻ B cells experiment per experiment is shown. ns: not significant.
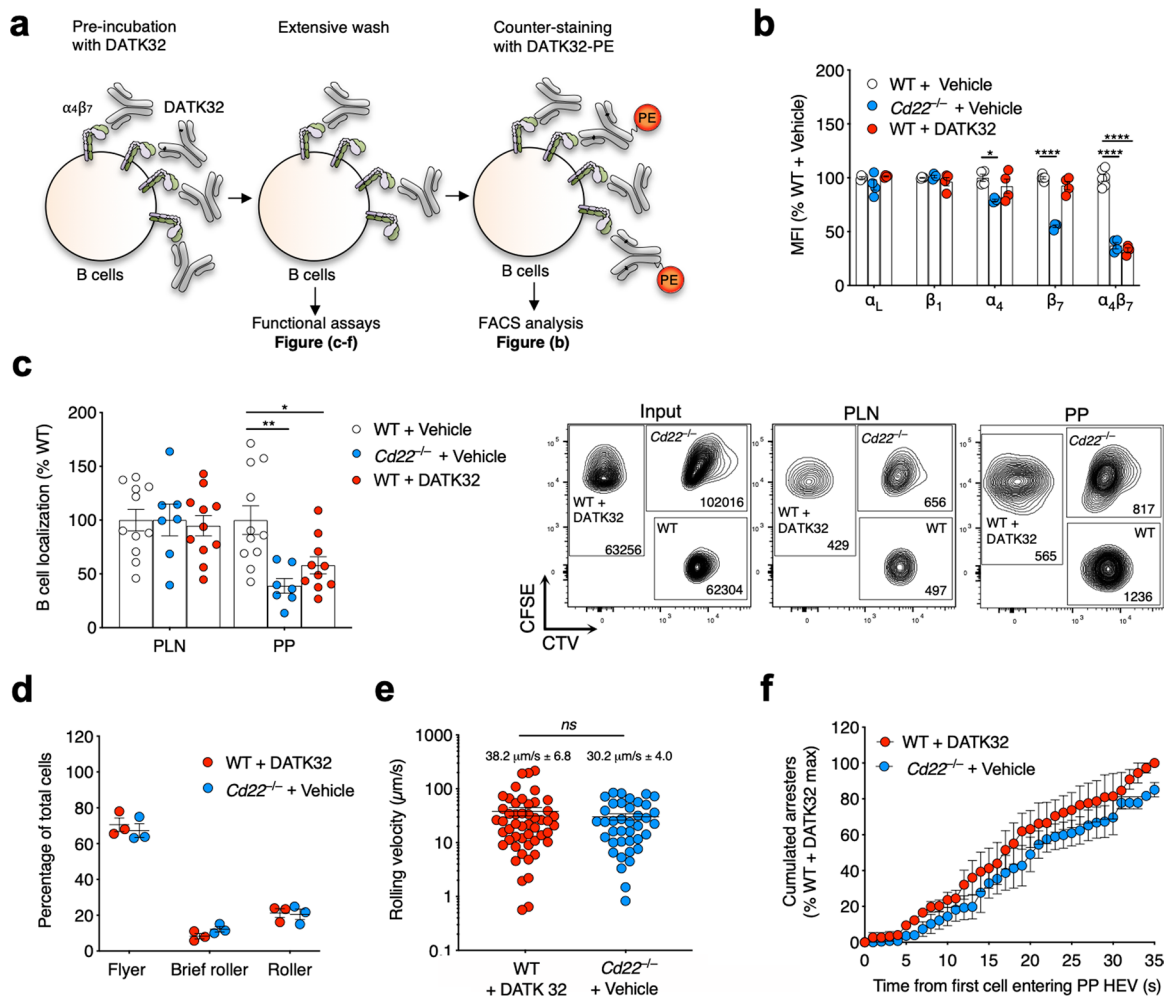
Extended Data Fig. 9 | WT B cells with reduced $\alpha_4\beta_7$ availability mimic the behavior of defective CD22-deficient B cell homing to PP. a, WT B cells were pre-incubated with inhibitory anti-$\alpha_4\beta_7$ Ab DATK32 (50 μg/mL) and washed extensively. DATK32-pretreated B cells were either counter-stained with Phyco-erythrin(PE)-conjugated DATK32 for flow cytometry analyses (**b**), or use in functional assays (**c-f**). **b**, Flow cytometry of WT + DATK32 vs. WT + Vehicle B cells stained for α_L, β_1, α_4, β_7, or $\alpha_4\beta_7$ presented as in Fig. 1. Shown are pooled data (mean ± SEM) from n = 2 independent experiments with 4 animals per group total. **c**, Localization of WT, $Cd22^{-/-}$, and WT + DATK32 B cells in PLN and PP after homing assays analyzed and presented as in Fig. 6. Shown are pooled data (mean ± SEM) of n = 3 experiments with 11 mice per group total. Representative dot plots gated in live naïve B cells are also shown including the number of cells within each gate. **d-f**, *In situ* video microscopy analyses of WT B cells + DATK32 vs. $Cd22^{-/-}$ B cells interactions with PP-HEVs analyzed and presented as in Fig. 6. Data represent the mean ± SEM of three independent experiments (**d,f**) and representative cells from all 3 experiments (**e**). Groups were compared using One-way ANOVA with Dunnett's multiple comparisons test (**b,c**), unpaired two-tailed Student's *t*-test (**d,e**), and paired two-tailed Student's *t*-test (**f**). *P ≤ 0.05, **P ≤ 0.01, and ****P ≤ 0.0001. ns: not significant.
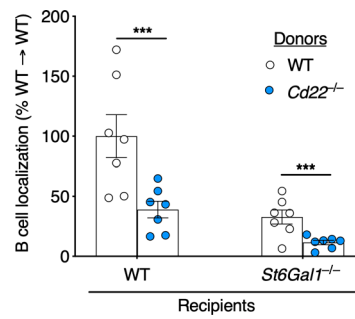
Extended Data Fig. 10 | Defective homing of CD22-deficient B cells in St6gal1-deficient recipient mice. Localization of WT and $Cd22^{-/-}$ B cells in the PPs of wild-type (WT) or ligand-deficient ($St6Gal1^{-/-}$) mice after short-term (1.5 hr) homing assays designed as in Fig. 6a. For each donor, the number of B cells isolated (Output) was normalized to the number of injected B cells (Input) and shown as a percentage of the WT → WT group mean. Shown are pooled data (mean ± SEM) from three experiments with n = 7 mice per group total. Groups were compared using two-tailed Student's t-test. ***P ≤ 0.001.

Corresponding author(s):   Dr. Romain Ballet and Prof. Eugene Butcher

Last updated by author(s):   May 6, 2020

Reporting Summary

Nature Research wishes to improve the reproducibility of the work that we publish. This form provides structure for consistency and transparency in reporting. For further information on Nature Research policies, see our Editorial Policies and the Editorial Policy Checklist.

Statistics

For all statistical analyses, confirm that the following items are present in the figure legend, table legend, main text, or Methods section.

n/a	Confirmed	
☐	☒	The exact sample size (n) for each experimental group/condition, given as a discrete number and unit of measurement
☐	☒	A statement on whether measurements were taken from distinct samples or whether the same sample was measured repeatedly
☐	☒	The statistical test(s) used AND whether they are one- or two-sided *Only common tests should be described solely by name; describe more complex techniques in the Methods section.*
☐	☒	A description of all covariates tested
☐	☒	A description of any assumptions or corrections, such as tests of normality and adjustment for multiple comparisons
☐	☒	A full description of the statistical parameters including central tendency (e.g. means) or other basic estimates (e.g. regression coefficient) AND variation (e.g. standard deviation) or associated estimates of uncertainty (e.g. confidence intervals)
☐	☒	For null hypothesis testing, the test statistic (e.g. F, t, r) with confidence intervals, effect sizes, degrees of freedom and P value noted *Give P values as exact values whenever suitable.*
☒	☐	For Bayesian analysis, information on the choice of priors and Markov chain Monte Carlo settings
☒	☐	For hierarchical and complex designs, identification of the appropriate level for tests and full reporting of outcomes
☒	☐	Estimates of effect sizes (e.g. Cohen's d, Pearson's r), indicating how they were calculated

Our web collection on statistics for biologists contains articles on many of the points above.

Software and code

Policy information about availability of computer code

Data collection	Flow Cytometry: BD FACSDIVA software (version 8.0.1) Confocal imaging: Zeiss Zen Black software In-situ videomicroscopy: Micro-Manager Open Source Microscopy Software
Data analysis	Flow Cytometry Analysis: FlowJo (V10.3) Image Processing: ImageJ (2.0.0-rc49/1.51d), Zeiss Zen, and Imaris (version 9) Data Analysis: Microsoft Office Excel (2011) Statistical Analysis: GraphPad Prism (V8)

For manuscripts utilizing custom algorithms or software that are central to the research but not yet described in published literature, software must be made available to editors and reviewers. We strongly encourage code deposition in a community repository (e.g. GitHub). See the Nature Research guidelines for submitting code & software for further information.

Data

Policy information about availability of data

All manuscripts must include a data availability statement. This statement should provide the following information, where applicable:
- Accession codes, unique identifiers, or web links for publicly available datasets
- A list of figures that have associated raw data
- A description of any restrictions on data availability

The data that support the findings of this study are available from the corresponding author upon request.

Field-specific reporting

Please select the one below that is the best fit for your research. If you are not sure, read the appropriate sections before making your selection.

☒ Life sciences ☐ Behavioural & social sciences ☐ Ecological, evolutionary & environmental sciences

For a reference copy of the document with all sections, see nature.com/documents/nr-reporting-summary-flat.pdf

Life sciences study design

All studies must disclose on these points even when the disclosure is negative.

Sample size	No sample size power calculation was performed. A minimum of 3 individual mice (biological replicates) were used for each experiment. Sample size of each experiment reflects the number of biological replicates deemed necessary to observe significant differences, if any, between genotypes. All details for each experiment is included in the corresponding figure legend.
Data exclusions	No data were excluded.
Replication	All attempts at replication were successful. Results from all experiments described were repeated in at least 2 (usually 3 or greater) independent experiments.
Randomization	Mice of similar age and sex were used for all the experiments reported. Animals were allocated to groups based on their genotype.
Blinding	Most of the acquisition and analysis were not blinded but kept as unbiased as possible: - For all flow cytometry, confocal microscopy and biochemistry studies, every sample/animal was processed identically by one experimenter to avoid any technical bias. For example, all tissue dissociation and staining were performed by the same researcher who processed each sample the same way. CTB injections or rotavirus inoculations were performed by the same researcher to ensure reproducible injections/inoculations from mouse to mouse and group to group. - For homing assay studies and in situ video-microscopy studies, cells from different groups were stained with different dyes, and we switch the dye allocation for each experiment, in addition to confirming that the dyes and concentrations used did not affect the behavior of the cells. - For each studies, we also include the appropriate internal controls and normalization methods to control for internal sample bias (please refer to the Methods). For example, normalization to Beta7 levels in Endocytosis/Biochemistry studies; staining each individual sample with the appropriate Isotype controls in flow cytometry studies; normalization of output data to input data for homing/in situ video-microscopy studies. - For in situ microscopy studies, data were analyzed in a blinded manner: cells were color coded and the researcher doing the analysis was unaware of the sample allocation. All conclusions were made based on statistical significance of the data.

Reporting for specific materials, systems and methods

We require information from authors about some types of materials, experimental systems and methods used in many studies. Here, indicate whether each material, system or method listed is relevant to your study. If you are not sure if a list item applies to your research, read the appropriate section before selecting a response.

Materials & experimental systems

n/a	Involved in the study
☐	☒ Antibodies
☒	☐ Eukaryotic cell lines
☒	☐ Palaeontology and archaeology
☐	☒ Animals and other organisms
☒	☐ Human research participants
☒	☐ Clinical data
☒	☐ Dual use research of concern

Methods

n/a	Involved in the study
☒	☐ ChIP-seq
☐	☒ Flow cytometry
☒	☐ MRI-based neuroimaging

Antibodies

Antibodies used	Antibody description, clone, catalog number, source, application, dilution: - Allophycocyanin-conjugated anti-mouse CD4, clone RM4-5, Cat# 100516, Biolegend, Flow cytometry, 1:200 - Phycoerythrin-indotricarbocyanine-conjugated anti-mouse CD3ε, clone 145-2C11, Cat# 100320, Biolegend, Flow cytometry, 1:200 - Peridinin-chlorophyll protein-Cyanine 5.5-conjugated anti-mouse IgD, clone 11.26c.2a, Cat# 405710, Biolegend, Flow cytometry, 1:100 - Phycoerythrin-conjugated anti-mouse CD19, clone 6D5, Cat# 115508, Biolegend, Flow cytometry, 1:200 - Brilliant violet 421-conjugated anti-mouse CD4, clone RM4-5, Cat # 100563, Biolegend, Flow cytometry, 1:200 - Phycoerythrin-conjugated anti-mouse CD49d, clone 9C10, Cat# 103705, Biolegend, Flow cytometry, 1:50

- Phycoerythrin-conjugated anti-mouse CD18, clone M18/2, Cat# 101407, Biolegend, Flow cytometry, 1:50
- Phycoerythrin-conjugated anti-mouse CD29, clone HM β1-1, Cat# 102207, Biolegend, Flow cytometry, 1:50
- Phycoerythrin-conjugated armenian hamster IgG isotype control, clone
HTK888, Cat# 400908, Biolegend, Flow cytometry, 1:50
- Phycoerythrin-conjugated anti-mouse CD71, clone RI7217, Cat# 113807, Biolegend, Flow cytometry, 1:50
- Purified anti rat/mouse CD29, clone HM β1-1, Cat# 102201, Biolegend, conjugated to pHrodo Red (Thermo), Flow cytometry, 1:35 (from 1 mg/ml stock)
- Purified rat IgG2a, k Isotype Control, clone RTK2758, Cat# 400501, Biolegend, used conjugated to pHrodo Red (Thermo), Flow cytometry, 1:35 (from 1 mg/ml stock)
- Phycoerythrin-conjugated rat IgG2a,κ isotype control, clone R35-95, Cat# 557229, BD Biosciences, Flow Cytometry, 1:50
- Phycoerythrin-conjugated anti-mouse CD11a, clone 2D7, Cat# 553121, BD Biosciences, Flow cytometry, 1:100
- Phycoerythrin-conjugated anti-mouse CD29, clone HM β1-1, Cat# 562801, BD Biosciences, Flow cytometry, 1:50
- Phycoerythrin-conjugated anti-mouse integrin β7, Cat# 557498, clone M293, BD Biosciences, Flow cytometry, 1:50
- Phycoerythrin-conjugated anti-mouse LPAM-1, Cat# 553811, clone DATK32, BD Biosciences, Flow cytometry 1:50
- Purified rat anti-mouse CD16/CD32, clone 2.4G2, Cat# 553142, BD Biosciences, Flow cytometry, 1:200
- Allophycocyanin-cyanine 7 rat anti-mouse CD19, clone 1D3, Cat# 557655, BD Biosciences, Flow cytometry, 1:100
- Purified Mouse Anti-Phosphotyrosine, clone PY20, Cat# 610000, BD Biosciences, Western blot, 1:2,000
- Fluorescein isothiocyanate-conjugated anti-mouse CD19, clone 1D3, Cat # 11-0193-81, eBiosciences, Flow cytometry, 1:100
- Fluorescein isothiocyanate-conjugated anti-mouse IgD, clone 11-26, Cat #11-5993-82, eBiosciences, Flow cytometry, 1:100
- Allophycocyanin-conjugated anti-mouse CD3e, clone 145-2C11, Cat# 17-0031-82, eBiosciences, Flow cytometry 1:200
- Purified anti-mouse/human integrin β7, clone FIB504, Cat# BE0062, BioXcell, used conjugated to pHrodo Red (Thermo), Flow cytometry, 1:35 (from 1 mg/mL stock)
- Purified mouse anti-mouse CD22, clone Cy34.1, Cat # BE0011, BioXCell, Proximity ligation assay, 1:500
- Polyclonal goat anti-mouse integrin β7, Cat. number AF3060, R&D Systems, Proximity ligation assay, 1:100
- Polyclonal goat anti-mouse integrin β1, Cat. Number AF2405, R&D Systems, Proximity ligation assay, 1:100
- Horseradish peroxidase-conjugated anti-mouse IgA, Cat. number: 5220-0367, SeraCare, ELISA/ELISPOT, 1:1,000
- Horseradish peroxidase-conjugated anti-mouse IgG, Cat. Number 5220-0339, SeraCare, ELISA/ELISPOT, 1:10,000-1:20,000
- Purified anti-mouse IgA, IgG, IgM polyclonal antibodies, Cat. number 5210-0187, SeraCare, ELISA/ELISPOT, 1:250
- Horseradish peroxidase-conjugated goat anti-rabbit IgG, Cat. number 31463, Thermo, ELISA, 1:30,000
- Purified rat anti-mouse α4β7, clone DATK32, Home-made, Functional assays, 50 µg/mL
- Purified rat anti-mouse β7, clone FIB504, Home-made, Immunoblot and immunoprecipitation, 10 µg/mL
- Purified rat anti-mouse α4, clone PS/2, Home-made, Proximity ligation assay, 20 µg/mL
- Guinea pig anti-rotavirus and Rabbit anti-rotavirus hyperimmune sera, produced by Quality Controlled Biochemicals after immunization of guinea pig and rabbit with RRV TLP and RRV DLP respectively, gifts from Professor Harry Greenberg, ELISA, 1:4,000
- Biotin-conjugated mouse anti-mouse CD22, clone Cy34.1, Cat. number 553382, BD Biosciences, IHC, 5µg/mL
- Rabbit anti-human/mouse Shp1, Cat. number PA5-27803, Invitrogen, IHC, 10µg/mL
- Alexa Fluor® 594-conjugated streptavidin, Cat. Number 405240, Biolegend, IHC, 2.5µg/mL
- Alexa Fluor® 594-conjugated donkey anti-rabbit, Cat. Number 711-586-152, Jackson ImmunoResearch, IHC, 1:400
- Alexa Fluor® 488-conjugated donkey anti-goat, Cat. Number 705-546-147, Jackson ImmunoResearch, IHC, 1:200
- Alexa Fluor 647®-conjugated streptavidin, Cat. number 016-600-084, Jackson ImmunoResearch, IHC, 1:200
- Horseradish peroxidase-conjugated goat anti-rat, Cat. number 405405, Biolegend, Immunoblot, 1:2,000
- Horseradish peroxidase-conjugated goat anti-mouse, Cat. number 405306, Biolegend, Immunoblot, 1:2,000

Validation

Antibodies used came from commercial vendors or were purified from in-house hybridomas.

First, we have thoroughly selected all our commercially available antibodies from commercial sources based on the validation provided by the manufacturer for the indicated species (i.e. mouse for our studies) and for the application(s) they sell the antibody for (i.e. either Flow Cytometry, IHC, immunoprecipitation, or immunoblot in our studies). Any information regarding the validation performed by the manufacturer can be retrieved on the manufacturers' websites using the informations that we provided in the "Antibodies used" section above.

For each antibody, the dilution was thoroughly optimized in the lab prior to its use in this study. We started with the dilution recommended by the manufacturer and then further optimized each dilution using appropriate Isotype control, single stains, sometimes buying and comparing different antibodies (e.g. Shp1, CD22, and Beta7 antibodies used for IHC), simultaneous analysis of cell populations of known phenotype, and whenever possible knock-out cells for the molecule of interest (e.g. Cd22 knock-out or viable motheathen mice in our studies).

For in-house hybridomas, antibodies were previously used for similar application. For example, we used the clone FIB504 for Beta7 immunoprecipitation and immunoblot studies as already previously described (Sun et al, Developmental Cell, 2014) and after comparing the FIB504 clone for IP/immunoblot to all the otherFIB clones we generated and characterized in the past (i.e. FIB21 FIB22, FIB27, FIB30, see Andrew et al, J. Immunol, 1994). We used the clone PS/2 to target the alpha4 integrin in PLA studies and the clone DATK32 to block the alpha4beta7 integrin for functional assays as described before (Hamann et al, J. Immunol, 1994).

Animals and other organisms

Policy information about studies involving animals; ARRIVE guidelines recommended for reporting animal research

Laboratory animals

Mouse strains used: C57BL/6 wild-type mice, BALB/c wild-type mice, CD22 knock-out mice, and St6Gal1 knock-out mice, were bred and housed in the animal facilities of the Veterans Affairs Palo Alto Health Care System, accredited by the Association for Assessment and Accreditation of Laboratory Animal Care. CD22 Y2,5,6F mice and CD22 R130E mice were bred and housed at the Department of Biology of the University of Erlangen; Ptpn6 meV/meV and Ptpn6 +/meV mice were bred and housed at the University of California San Francisco. Unless otherwise stated, 6-12 weeks old male or female mice were used in all experiments.

Wild animals	The study did not involve wild animals
Field-collected samples	The study did not involve samples collected from the field
Ethics oversight	All animal work was approved by the Institutional Animal Care and Use Committee at the Veterans Affairs Palo Alto Health Care System, or by relevant animal care committees at the University of Erlangen.

Note that full information on the approval of the study protocol must also be provided in the manuscript.

Flow Cytometry

Plots

Confirm that:

☒ The axis labels state the marker and fluorochrome used (e.g. CD4-FITC).

☒ The axis scales are clearly visible. Include numbers along axes only for bottom left plot of group (a 'group' is an analysis of identical markers).

☒ All plots are contour plots with outliers or pseudocolor plots.

☒ A numerical value for number of cells or percentage (with statistics) is provided.

Methodology

Sample preparation	Single cell leukocyte suspension were prepared from freshly harvested spleen, peripheral lymph nodes, intestinal Peyer's patches, mesenteric lymph nodes, or bone marrow. For each organ, cells were isolated by pressing the tissue through 70um filter. For bone marrow, cell suspension were prepared by flushing the marrow with RPMI prior to pressing any cell aggregate through 70um filter. Red blood cells lysis was performed at room temperature for 5 minutes with commercially available lysis buffer. Single cell suspension were stained as described in the Methods, including incubation with Rat serum and Fc Block (anti CD16/32) for 5-15 minutes prior to incubation with antibody cocktails for an additional 30-45 minutes on ice. Freshly stained cells were analyzed immediately following preparation.
Instrument	BD Fortessa; BD LSR II
Software	Data collection: BDFACSDiva. Data analysis: FlowJo (V10.3)
Cell population abundance	Purity assessment: for each experiment involving purified B cells or CD4 T cells, a flow cytometry analysis of the isolated fraction was performed and purity consistently yielded 94-98%.
Gating strategy	Cell populations of interest (i.e. lymphocytes) were identified by cell size in a FSC-A vs. SSC-A plot. Single cells were discriminated in a FSC-H vs. FSC-W plot followed by SSC-H vs. FSC-W plot. DAPI was used to separate dead/dying cells from healthy cells. Within singlets live lymphocytes, naive B cells were defined as CD19+ IgD+ ; CD4 T cells as CD3+ CD4+; and CD8 T cells as CD3+ CD4-.

☒ Tick this box to confirm that a figure exemplifying the gating strategy is provided in the Supplementary Information.